Supplemental Material

Atrial Myocyte NLRP3/CaMKII Nexus Forms a Substrate for Post-Operative Atrial Fibrillation

Jordi Heijman, PhD[#]; Azinwi Phina Muna, PhD[#]; Tina Veleva, MD; Cristina E. Molina, PhD; Henry Sutanto, MD, MSc; Marcel Tekook, PhD; Qiongling Wang, PhD; Issam H. Abu-Taha, PhD; Marcel Gorka; Stephan Künzel, MD; Ali El-Armouche, MD; Hermann Reichenspurner, MD, PhD; Markus Kamler, MD; Viacheslav Nikolaev, PhD; Ursula Ravens, MD; Na Li, PhD; Stanley Nattel, MD; Xander H.T. Wehrens, MD, PhD; Dobromir Dobrev, MD

[#]These authors contributed equally

Corresponding Author:
Dobromir Dobrev, MD
Hufelandstr. 55, 45122 Essen, Germany
Phone: +49 201 723 3477, Fax: +49 201 723 5593
E-Mail: dobromir.dobrev@uk-essen.de.

Contents

Patient Characteristics

Right-atrial (RA) appendages were obtained from patients without a history of atrial fibrillation (AF) undergoing open heart surgery and were subsequently divided into a control group that did not develop post-operative AF (Ctl) and a group that developed post-operative AF (POAF). An overview of the clinical characteristics of all patients included in this study is provided in **Online Table I**. Clinical characteristics of the subsets of patients whose samples were used for cell isolation and patch-clamp recording, multicellular action potential (AP) recordings, or biochemical experiments are given in **Online Tables II, III and IV**, respectively. Samples from 2 Ctl patients and 3 POAF patients were employed for both cell isolation and biochemical experiments and are therefore included in both **Online Table II and IV**. Experimental protocols were approved by ethical review boards of University Hospital Essen (#12-5268-BO), University Medical Center Hamburg-Eppendorf (WF-088/18), and Dresden University of Technology (No: EK114082002) were conducted in accordance with the Declaration of Helsinki. Each patient gave written informed consent.

C-reactive protein (CRP) levels were determined as part of the routine clinical care at the central diagnostic laboratory of MVZLM Ruhr using Cobas C702, C-reactive Protein Generation 3 (Roche Diagnostics, Germany) from patient serum. The frequency and timing of CRP measurements was not standardized, but for patients included in the analysis, values were always available just prior to the surgery, on 2.1±0.9 out of the first 3 postoperative days, and on 3.3±1.4 days in the first week post-surgery.

Online Table I. Clinical characteristics of all patient samples employed in this study.

	Ctl (n=166)		POAF (n=99)		P-value
	Value	N	Value	N	Value
Demographics					
Age (years)	68 (57-75)	166	71 (62-78)	99	**0.036**
Female gender	53 (31.9%)	166	39 (39.4%)	99	0.217
BMI (kg / m2)	27 (25-30)	140	27 (24-31)	87	0.994
Indication for surgery					
CAD AVD/MVD CAD+AVD/MVD Other	64 (38.6%), 72 (43.4%), 26 (15.7%), 4 (2.4%)	166	30 (30.3%), 47 (47.5%), 21 (21.2%), 1 (1.0%)	99	0.370
Medical history					
Atrial fibrillation	0 (0.0%)	166	0 (0.0%)	99	>0.999
CKD	15 (13.3%)	113	16 (20.8%)	77	0.169
COPD	28 (19.7%)	142	16 (18.0%)	89	0.743
Dyslipidemia	78 (53.4%)	146	42 (47.7%)	88	0.398
Diabetes	49 (30.8%)	159	28 (29.2%)	96	0.781
Heart failure (NYHA) <II II III IV	 53 (36.8%) 30 (20.8%) 50 (34.7%) 11 (7.6%)	144	 29 (31.9%) 12 (13.2%) 42 (46.2%) 8 (8.8%)	91	0.244
Hypertension	117 (73.1%)	160	73 (76.0%)	96	0.606
Pulmonary hypertension	18 (15.7%)	115	13 (17.6%)	74	0.729
Sleep apnea	7 (5.2%)	134	2 (2.4%)	82	0.320
Lab					
eGFR (ml/min/1.73m^2)	74.0±20.2	147	67.9±21.1	91	**0.029**
Preoperative CRP (mg/dL)	0.3 (0.1-0.9)	76	0.4 (0.1-0.7)	50	0.629
Max postoperative CRP (mg/dL)	15.5±6.73	75	15.4±4.81	50	0.944
ECG					
RR (ms)	877 (786-971)	148	856 (751-944)	91	0.137
P-wave duration (ms)	94 (70-108)	113	97 (75-114)	66	0.360
PQ (ms)	160 (142-178)	113	164 (142-192)	68	0.199
QRS (ms)	92 (84-104)	114	90 (84-110)	75	0.859
QTc (ms)	432 (415-454)	148	437 (419-468)	91	0.156
Echocardiography					
LA diameter (mm)	41.2±6.25	119	41.2±5.83	82	0.938
LVEF (%)	60 (52-65)	153	60 (50-65)	91	0.269
Aortic valve insufficiency None Mild Moderate Severe	 66 (49.6%) 47 (35.5%) 19 (14.3%) 1 (0.8%)	133	 41 (50.0%) 29 (35.4%) 11 (13.4%) 1 (1.2%)	82	0.986
Mitral valve insufficiency None Mild Moderate Severe	 56 (41.5%) 61 (45.2%) 12 (8.9%) 6 (4.4%)	135	 26 (32.1%) 34 (42.0%) 13 (16.0%) 9 (11.1%)	81	0.080
Tricuspid valve insufficiency None Mild Moderate Severe	 96 (71.1%) 35 (25.9%) 4 (3.0%) 0 (0.0%)	135	 52 (63.4%) 23 (28.0%) 7 (8.5%) 0 (0.0%)	82	0.161

Medication					
ACE inhibitors or ARBs	102 (61.4%)	166	60 (60.6%)	99	0.892
Beta-blockers	100 (60.2%)	166	52 (52.5%)	99	0.219
Digitalis	4 (2.4%)	166	6 (6.1%)	99	0.131
Dihydropyridines	19 (11.4%)	166	19 (19.2%)	99	0.082
Diuretics	57 (34.3%)	166	44 (44.4%)	99	0.101
Lipid-lowering drugs	100 (60.2%)	166	49 (49.5%)	99	0.088
Nitrates	15 (9.0%)	166	13 (13.1%)	99	0.294

Continuous variables are presented as mean±SD for normal-distributed data or median and interquartile ranges. Categorical data are given as number of patients (%). Normal-distributed continuous data were compared using unpaired Student's *t*-test, non-normal-distributed continuous data using Mann-Whitney test, and categorical data using Chi-squared tests. Abbreviations: ACE, angiotensin-converting enzyme; ARB, angiotensin receptor blocker; AVD/MVD, aortic/mitral valve disease; BMI, body mass index; CAD, coronary artery disease; CKD, chronic kidney disease; COPD, chronic obstructive pulmonary disease; CRP, C-reactive protein; Dihydropyridines, dihydropyridine-type Ca^{2+}-channel blockers; ECG, electrocardiogram; eGFR, estimated glomerular filtration rate; LA, left atrium; LVEF, left ventricular ejection fraction; NYHA, New York Heart Association. N-numbers represent number of patients for which information on the corresponding clinical variable was available.

Online Table II. Clinical characteristics of patient samples employed for simultaneous patch-clamp/Ca^{2+}-imaging or perforated patch-clamp recordings in isolated atrial cardiomyocytes.

	Ctl (n=75)		POAF (n=44)		P-value
	Value	N	Value	N	Value
Demographics					
Age (years)	70 (56-75)	75	73 (62-78)	44	**0.040**
Female (%)	21 (28.0%)	75	21 (47.7%)	44	**0.030**
BMI (kg / m2)	28 (26-31)	50	27 (24-30)	32	0.177
Indication for surgery					
CAD AVD/MVD CAD+AVD/MVD Other	24 (32.0%) 34 (45.3%) 15 (20.0%) 2 (2.7%)	75	9 (20.5%) 25 (56.8%) 10 (22.7%) 0 (0.0%)	44	0.342
Medical history					
Atrial fibrillation	0 (0.0%)	75	0 (0.0%)	44	>0.999
CKD	4 (6.9%)	58	4 (10.5%)	38	0.529
COPD	6 (11.3%)	53	7 (19.4%)	36	0.287
Dyslipidemia	26 (47.3%)	55	17 (51.5%)	33	0.700
Diabetes	17 (25.0%)	68	10 (24.4%)	41	0.943
Heart failure (NYHA) <II II III IV	 19 (35.2%) 13 (24.1%) 19 (35.2%) 3 (5.6%)	54	 10 (27.8%) 6 (16.7%) 18 (50.0%) 2 (5.6%)	36	0.555
Hypertension	40 (58.0%)	69	29 (70.7%)	41	0.181
Pulmonary hypertension	3 (7.1%)	42	6 (21.4%)	28	0.080
Sleep apnea	3 (6.7%)	45	1 (3.7%)	27	0.595
Lab					
eGFR (ml/min/1.73m^2)	72.1±22.9	58	69.8±20.3	37	0.625
Preoperative CRP (mg/dL)	0.3 (0.1-0.8)	45	0.2 (0.1-0.5)	27	0.758
Max postoperative CRP (mg/dL)	16.0±6.73	45	15.4±4.21	27	0.669
ECG					
RR (ms)	891 (814-969)	58	842 (747-926)	36	0.053
P-wave duration (ms)	85.5±25.5	57	86.7±26.9	32	0.849
PQ (ms)	158 (138-174)	57	163 (142-188)	32	0.363
QRS (ms)	90 (80-102)	58	89 (80-105)	36	0.852
QTc (ms)	426 (402-447)	58	438 (423-454)	36	**0.019**
Echocardiography					
LA diameter (mm)	40.0±6.51	59	40.8±5.83	38	0.511
LVEF (%)	60 (55-65)	65	60 (53-65)	38	0.687
Aortic valve insufficiency None Mild Moderate Severe	 14 (31.8%) 21 (47.7%) 8 (18.2%) 1 (2.3%)	44	 12 (44.4%) 11 (40.7%) 4 (14.8%) 0 (0.0%)	27	0.651
Mitral valve insufficiency None Mild Moderate Severe	 18 (40.0%) 24 (53.3%) 2 (4.4%) 1 (2.2%)	45	 5 (19.2%) 13 (50.0%) 5 (19.2%) 3 (11.5%)	26	**0.038**

Tricuspid valve insufficiency None Mild Moderate Severe	 30 (66.7%) 14 (31.1%) 1 (2.2%) 0 (0.0%)	45	 15 (55.6%) 11 (40.7%) 1 (3.7%) 0 (0.0%)	27	0.632
Medication					
ACE inhibitors or ARBs	38 (50.7%)	75	24 (54.5%)	44	0.683
Beta-blockers	31 (41.3%)	75	19 (43.2%)	44	0.844
Digitalis	0 (0.0%)	75	0 (0.0%)	44	>0.999
Dihydropyridines	8 (10.7%)	75	3 (6.8%)	44	0.484
Diuretics	23 (30.7%)	75	18 (40.9%)	44	0.256
Lipid-lowering drugs	38 (50.7%)	75	21 (47.7%)	44	0.757
Nitrates	6 (8.0%)	75	3 (6.8%)	44	0.814

Continuous variables are presented as mean±SD for normal-distributed data or median and interquartile ranges. Categorical data are given as number of patients (%). Normal-distributed continuous data were compared using unpaired Student's *t*-test, non-normal-distributed continuous data using Mann-Whitney test, and categorical data using Chi-squared tests. Abbreviations: ACE, angiotensin-converting enzyme; ARB, angiotensin receptor blocker; AVD/MVD, aortic/mitral valve disease; BMI, body mass index; CAD, coronary artery disease; CKD, chronic kidney disease; COPD, chronic obstructive pulmonary disease; CRP, C-reactive protein; Dihydropyridines, dihydropyridine-type Ca^{2+}-channel blockers; ECG, electrocardiogram; eGFR, estimated glomerular filtration rate; LA, left atrium; LVEF, left ventricular ejection fraction; NYHA, New York Heart Association. N-numbers represent number of patients for which information on the corresponding clinical variable was available.

Online Table III. Clinical characteristics of patient samples employed for multicellular action potential recordings.

	Ctl (n=34)		POAF (n=16)		P-value
	Value	N	Value	N	Value
Demographics					
Age (years)	69.3±9.81	34	71.1±7.89	16	0.518
Female gender	13 (38.2%)	34	6 (37.5%)	16	0.960
BMI (kg / m2)	27.1±3.30	34	28.1±3.92	16	0.378
Indication for surgery					
CAD	23 (67.6%)	34	7 (43.8%)	16	0.264
AVD/MVD	8 (23.5%)		7 (43.8%)		
CAD+AVD/MVD	3 (8.8%)		2 (12.5%)		
Other	0 (0.0%)		0 (0.0%)		
Medical history					
Atrial fibrillation	0 (0.0%)	34	0 (0.0%)	16	>0.999
CKD		0		0	
COPD	13 (38.2%)	34	4 (25.0%)	16	0.357
Dyslipidemia	23 (67.6%)	34	10 (62.5%)	16	0.720
Diabetes	10 (29.4%)	34	4 (25.0%)	16	0.746
Heart failure (NYHA)		34		16	0.814
<II	11 (32.4%)		4 (25.0%)		
II	0 (0.0%)		0 (0.0%)		
III	18 (52.9%)		10 (62.5%)		
IV	5 (14.7%)		2 (12.5%)		
Hypertension	32 (94.1%)	34	15 (93.8%)	16	0.959
Pulmonary hypertension	9 (26.5%)	34	2 (12.5%)	16	0.266
Sleep apnea	2 (5.9%)	34	0 (0.0%)	16	0.322
Lab					
eGFR (ml/min/1.73m^2)	80 (72-89)	33	80 (67-87)	16	0.773
Preoperative CRP (mg/dL)		0		0	
Max postoperative CRP (mg/dL)		0		0	
ECG					
RR (ms)	959±165	34	945±156	16	0.782
P-wave duration (ms)		0		0	
PQ (ms)		0		0	
QRS (ms)		0		0	
QTc (ms)	427±24.9	34	425±34.5	16	0.746
Echocardiography					
LA diameter (mm)	43.2±5.68	27	41.7±5.97	14	0.456
LVEF (%)	56.5±11.5	34	53.9±15.5	16	0.513
Aortic valve insufficiency		34		16	0.470
None	17 (50.0%)		9 (56.2%)		
Mild	14 (41.2%)		7 (43.8%)		
Moderate	3 (8.8%)		0 (0.0%)		
Severe	0 (0.0%)		0 (0.0%)		
Mitral valve insufficiency		34		16	0.999
None	10 (29.4%)		5 (31.3%)		
Mild	17 (50.0%)		8 (50.0%)		
Moderate	5 (14.7%)		2 (12.5%)		
Severe	2 (5.9%)		1 (6.3%)		

Tricuspid valve insufficiency None Mild Moderate Severe	 27 (79.4%) 5 (14.7%) 2 (5.9%) 0 (0.0%)	34	 12 (75.0%) 2 (12.5%) 2 (12.5%) 0 (0.0%)	16	0.719
Medication					
ACE inhibitors or ARBs	30 (88.2%)	34	12 (75.0%)	16	0.234
Beta-blockers	29 (85.3%)	34	13 (81.3%)	16	0.716
Digitalis	1 (2.9%)	34	1 (6.3%)	16	0.578
Dihydropyridines	4 (11.8%)	34	3 (18.8%)	16	0.507
Diuretics	15 (44.1%)	34	8 (50.0%)	16	0.697
Lipid-lowering drugs	30 (88.2%)	34	11 (68.8%)	16	0.094
Nitrates	5 (14.7%)	34	2 (12.5%)	16	0.834

Continuous variables are presented as mean±SD for normal-distributed data or median and interquartile ranges. Categorical data are given as number of patients (%). Normal-distributed continuous data were compared using unpaired Student's *t*-test, non-normal-distributed continuous data using Mann-Whitney test, and categorical data using Chi-squared tests. Abbreviations: ACE, angiotensin-converting enzyme; ARB, angiotensin receptor blocker; AVD/MVD, aortic/mitral valve disease; BMI, body mass index; CAD, coronary artery disease; CKD, chronic kidney disease; COPD, chronic obstructive pulmonary disease; CRP, C-reactive protein; Dihydropyridines, dihydropyridine-type Ca^{2+}-channel blockers; ECG, electrocardiogram; eGFR, estimated glomerular filtration rate; LA, left atrium; LVEF, left ventricular ejection fraction; NYHA, New York Heart Association. N-numbers represent number of patients for which information on the corresponding clinical variable was available.

Online Table IV. Clinical characteristics of patient samples employed for biochemical experiments.

	Ctl (n=59)		POAF (n=42)		P-value
	Value	N	Value	N	Value
Demographics					
Age (years)	66 (56-75)	59	69 (61-77)	42	0.109
Female (%)	19 (32.2%)	59	14 (33.3%)	42	0.905
BMI (kg / m2)	26 (24-30)	59	27 (22-31)	42	0.929
Indication for surgery					
CAD AVD/MVD CAD+AVD/MVD Other	17 (28.8%) 32 (54.2%) 8 (13.6%) 2 (3.4%)	59	14 (33.3%) 17 (40.5%) 10 (23.8%) 1 (2.4%)	42	0.449
Medical history					
Atrial fibrillation	0 (0.0%)	59	0 (0.0%)	42	>0.999
CKD	11 (19.0%)	58	12 (28.6%)	42	0.260
COPD	9 (15.5%)	58	5 (12.5%)	40	0.675
Dyslipidemia	32 (54.2%)	59	15 (35.7%)	42	0.066
Diabetes	22 (37.3%)	59	14 (33.3%)	42	0.683
Heart failure (NYHA) <II II III IV	 25 (42.4%) 17 (28.8%) 14 (23.7%) 3 (5.1%)	59	 17 (40.5%) 6 (14.3%) 15 (35.7%) 4 (9.5%)	42	0.239
Hypertension	47 (79.7%)	59	31 (73.8%)	42	0.489
Pulmonary hypertension	6 (14.6%)	41	5 (15.2%)	33	0.950
Sleep apnea	2 (3.4%)	58	2 (4.8%)	42	0.741
Lab					
eGFR (ml/min/1.73m^2)	72.0±18.6	59	61.9±19.8	41	**0.012**
Preoperative CRP (mg/dL)	0.3 (0.1-0.9)	34	0.4 (0.1-1.0)	26	0.638
Max postoperative CRP (mg/dL)	14.8±6.42	33	14.8±5.48	26	0.985
ECG					
RR (ms)	815±161	59	813±124	42	0.953
P-wave duration (ms)	94.9±24.0	59	98.1±27.3	37	0.551
PQ (ms)	164 (147-180)	59	164 (146-210)	39	0.500
QRS (ms)	96 (86-106)	59	91 (84-117)	42	0.639
QTc (ms)	442 (425-470)	59	442 (422-471)	42	0.807
Echocardiography					
LA diameter (mm)	41.8±5.74	34	41.2±5.63	33	0.945
LVEF (%)	60 (50-65)	55	55 (43-64)	39	0.250
Aortic valve insufficiency None Mild Moderate Severe	 36 (62.1%) 13 (22.4%) 9 (15.5%) 0 (0.0%)	58	 22 (52.4%) 12 (28.6%) 7 (16.7%) 1 (2.4%)	42	0.593
Mitral valve insufficiency None Mild Moderate Severe	 29 (49.2%) 21 (35.6%) 6 (10.2%) 3 (5.1%)	59	 15 (35.7%) 14 (33.3%) 6 (14.3%) 7 (16.7%)	42	0.193

Tricuspid valve insufficiency None Mild Moderate Severe	 41 (69.5%) 17 (28.8%) 1 (1.7%) 0 (0.0%)	59	 26 (61.9%) 12 (28.6%) 4 (9.5%) 0 (0.0%)	42	0.197
Medication					
ACE inhibitors or ARBs	34 (57.6%)	59	25 (59.5%)	42	0.849
Beta-blockers	43 (72.9%)	59	21 (50.0%)	42	**0.019**
Digitalis	3 (5.1%)	59	5 (11.9%)	42	0.211
Dihydropyridines	8 (13.6%)	59	13 (31.0%)	42	**0.034**
Diuretics	21 (35.6%)	59	20 (47.6%)	42	0.225
Lipid-lowering drugs	34 (57.6%)	59	17 (40.5%)	42	0.089
Nitrates	3 (5.1%)	59	8 (19.0%)	42	**0.026**

Continuous variables are presented as mean±SD for normal-distributed data or median and interquartile ranges. Categorical data are given as number of patients (%). Normal-distributed continuous data were compared using unpaired Student's *t*-test, non-normal-distributed continuous data using Mann-Whitney test, and categorical data using Chi-squared tests. Abbreviations: ACE, angiotensin-converting enzyme; ARB, angiotensin receptor blocker; AVD/MVD, aortic/mitral valve disease; BMI, body mass index; CAD, coronary artery disease; CKD, chronic kidney disease; COPD, chronic obstructive pulmonary disease; CRP, C-reactive protein; Dihydropyridines, dihydropyridine-type Ca^{2+}-channel blockers; ECG, electrocardiogram; eGFR, estimated glomerular filtration rate; LA, left atrium; LVEF, left ventricular ejection fraction; NYHA, New York Heart Association. N-numbers represent number of patients for which information on the corresponding clinical variable was available.

Experimental Methods

Sharp-electrode AP-recordings

Free-running atrial trabeculae (<1 mm in diameter and 2–5 mm in length) were dissected from RA appendages and mounted on the bottom of a 5-mL organ bath perfused with 50-mL of recirculating, oxygenized Tyrode's solution (flow rate 7 mL/min, temperature 36±1°C. The bath solution contained (in mmol/L): NaCl 127, KCl 4.5, $MgCl_2$ 1.5, $CaCl_2$ 1.8, glucose 10, $NaHCO_3$ 22, and NaH_2PO_4 0.42 and was equilibrated with 5% CO_2 in O_2 (pH=7.4). APs were recorded as previously described.[21,60] Preparations were electrically stimulated at a basal rate of 1-Hz with isolated square-wave stimuli of 1-ms duration, 2 times threshold intensity. After a 60-min equilibration period, transmembrane potentials were recorded with glass microelectrodes filled with 2.5 M KCl. Tip resistances of the electrodes were between 20 and 80 MΩ. Both timing of the driving stimuli and pre-processing of the transmembrane potential responses were carried out with dedicated software for AP recordings, as previously described.[60]

Perforated patch-clamp experiments

Total membrane current was measured in atrial cardiomyocytes at room temperature using the whole-cell perforated-patch configuration with an EPC-10 amplifier (HEKA Elektronik, Germany), as previously described.[22,61] Membrane capacitance was 61.4±24.8 pF in Ctl (n=37/30) vs. 56.0±21.8 pF in POAF (n=27/17; P=0.403) and currents were corrected for membrane capacitance. The extracellular solution contained (in mmol/L): NaCl 127, TEA 5, HEPES 10, $NaHCO_3$ 4, NaH_2PO_4 0.33, glucose 10, pyruvic acid 5, $CaCl_2$ 2, $MgCl_2$ 1.8 (pH=7.4) and the pipette solution contained (in mmol/L): aspartic acid 109, CsCl 47, Mg_2ATP 3, $MgCl_2$ 1, Na_2-phosphocreatine 5, Li_2GTP 0.42, HEPES 10 (pH=7.2 with CsOH). Amphotericin-B (250-mg/mL) was added to the pipette solution before starting an experiment. All chemicals were acquired from Sigma-Aldrich. The pipette resistance was 2-5 MΩ.

L-type Ca^{2+}-current ($I_{Ca,L}$) was measured during a 200-ms depolarizing pulse to 0 mV following a prepulse from -80 to -45 mV to inactivate the Na^+-current at 0.5-Hz. $I_{Ca,L}$ amplitude was determined as the difference between the peak inward current and the current at the end of the depolarization step. The time constants of $I_{Ca,L}$ inactivation were determined from a bi-exponential fit of the decaying phase of $I_{Ca,L}$. The $I_{Ca,L}$ voltage dependence was determined using test potentials between -40 and +50 mV and voltage dependence of inactivation was assessed using 300-ms inactivating pulses to potentials from -50 to 0 mV followed by a test pulse to 0 mV. Subsequently, the mid-point (V_{mid}) of inactivation was determined by fitting a Boltzmann curve [$I = 1 / (1 + \exp((V - V_{mid})/k))$] to the $I_{Ca,L}$ amplitude vs. inactivating potential curve. Recovery of $I_{Ca,L}$ from inactivation was assessed using a two-pulse protocol with increasing intervals at – 80 mV between the first and the second pulse used to elicit $I_{Ca,L}$ and was quantified using a mono-exponential fit of the individual recovery curves.

Sarcoplasmic reticulum (SR) Ca^{2+}-content was measured as the integrated Na^+/Ca^{2+}-exchanger (NCX)-mediated current (I_{NCX}) during caffeine application (10-mmol/L) to empty the SR and spontaneous SR Ca^{2+}-release events (SCaEs) were quantified as the frequency of transient-inward I_{NCX} at holding potentials of -50 and -80 mV.[22,12]

Ruptured patch-clamp experiments with simultaneous $[Ca^{2+}]_i$ recording

Intracellular $[Ca^{2+}]$ was quantified at 37ºC using Fluo-3-acetoxymethyl ester (Fluo-3 AM, Invitrogen, Carlsbad, CA) in both bath and pipette solutions, as previously described.[6,7] After 10-min loading with 10-µmol/L Fluo-3 and 30 min de-esterification, fluorescence was excited at 488 nm and emitted light (>520 nm) was recorded. Fluorescence intensity was converted to $[Ca^{2+}]_i$ using $[Ca^{2+}]_i = k_d * F / (F_{max} – F)$, where k_d is the dissociation constant of Fluo-3 (864-nmol/L), F is baseline-corrected Fluo-3 fluorescence, and F_{max} is baseline-corrected, Ca^{2+}-saturated fluorescence obtained at the end of each experiment.[10,11] In a subset of experiments, results were presented as relative fluorescence changes (F/F_0) obtained at room temperature. Simultaneously, membrane currents were recorded in whole-cell ruptured-patch configuration under voltage-clamp conditions. Membrane capacitance was 79.4 (56.9-125.9) pF in Ctl (n=78/42) vs. 101.8 (64.9-134.0) pF in POAF (n=46/25; *P*=0.387) and currents were corrected for membrane capacitance (expressed as pA/pF). Borosilicate glass microelectrodes had tip resistances of 2-5 MΩ when filled with pipette solution, containing (in mmol/L): EGTA 0.02, Fluo-3 0.1, GTP-Tris 0.1, HEPES 10, K-aspartate 92, KCl 48, Mg-ATP 1, Na_2-ATP 4 (pH=7.2). Seal-resistances were 4-8 GΩ. Series resistance and cell capacitance were compensated. During experiments, myocytes were superfused with a bath solution containing (in mmol/L): $CaCl_2$ 2, glucose 10, HEPES 10, KCl 4, $MgCl_2$ 1, NaCl 140, probenecid 2 (pH=7.4). K^+-currents were blocked with 4-aminopyridine (5-mmol/L) and $BaCl_2$ (0.1-mmol/L). Drugs were applied via a rapid solution exchange system (ALA Scientific Instruments, Long Island, NY). pClamp-Software (V10.2, Molecular Devices, Sunnyvale, CA) was used for data acquisition and analysis.

$I_{Ca,L}$ and corresponding Ca^{2+} transients (CaT) were activated using consecutive 100-ms depolarizing steps to +10 mV, preceded by a 100-ms ramp-pulse from a holding potential of -80 mV to -40 mV to inactivate Na^+ currents, delivered at a rate of 0.5-Hz. Caffeine (10-mmol/L) was used for rapid depletion and quantification of SR Ca^{2+}-content as amplitude of caffeine-induced CaT or integrated I_{NCX}. SR Ca^{2+} leak was measured as the decrease in $[Ca^{2+}]_i$ following application of tetracaine (1-mmol/L) in the absence of extracellular Ca^{2+}/Na^+, as described by Shannon et al.[36] SERCA activity was determined as the difference in the rate constants of the $I_{Ca,L}$-triggered CaT decay (mediated by SERCA, NCX and the plasmalemmal Ca^{2+}-ATPase) and the rate constants of the caffeine-induced CaT decay (reflecting Ca^{2+} extrusion via NCX and the plasmalemmal Ca^{2+}-ATPase only) based on a mono-exponential fit in the same cardiomyocyte.[10,11] SCaEs were analyzed prior to tetracaine application during 0-mmol/L extracellular Ca^{2+}/Na^+ and during acute application of interleukin (IL)-1β (40-ng/mL) in the presence of 5-mmol/L extracellular Ca^{2+} at a holding potential of -80 mV. SCaEs were detected using custom Matlab (Mathworks, Natick, MA) software as local maxima exceeding 10% of the CaT amplitude in a low-pass filtered (40-ms average) version of the fluorescence signal and SCaE incidence was normalized to recording length. SCaE detection was visually confirmed by one of the investigators.

Only striated, Ca^{2+}-tolerant cells with clear membrane delineation were used for patch-clamp analyses. Cells were excluded from analysis in case of incomplete (due to cardiomyocyte death) or unstable recordings (increasing leak, varying seal resistance, unsuccessful caffeine application, artifacts due to cell contraction or debris). The number of recordings excluded for different reasons for all experiments are indicated in **Online Figure I**.

Preparation of cardiomyocyte-enriched fractions

Cardiomyocyte-enriched fractions were obtained from human atrial samples using bovine serum albumin (BSA)-gradient filtration, as previously described.[26] In brief, isolated cells obtained after collagenase/protease digestion and centrifugation of right-atrial tissue samples were re-suspended at room temperature in Ca^{2+}-free Tyrode's solution containing 0.1% BSA. Cell suspensions were pooled, layered over a 6% BSA gradient and allowed to sediment for 45 min.[26] Cell debris and undigested tissue fragments were largely located in the upper part of the 6% BSA fraction, whereas non-cardiomyocytes (fibroblasts, etc.), were mainly retained at the phase boundary between 0.1% and 6% BSA. Atrial cardiomyocytes (rod-shaped, striated) were enriched at the bottom of the gradient, as verified by light microscopy and cardiomyocyte-enriched fractions are negative for the specific macrophage/eosinophilic-granulocyte marker F4/80.[26,18] Dog atrial cardiomyocyte- and atrial fibroblast-enriched fractions were obtained from atrial tissue available from prior studies in male and female control mongrel dogs (n=4) or mongrel dogs with atrial tachycardia-related remodeling (atrial tachypacing at 600 bpm for 1 week; n=2) of unknown age (Laka Inc., Montreal, CA), as previously described.[62,63] Animal care procedures were approved by the Animal Research Ethics Committee of the Montreal Heart Institute. After ketamine (5.3 mg/kg, intravenously)/diazepam (0.25 mg/kg, intravenously)/1.5% isoflurane anesthesia, atrial tachycardia-related remodeling dogs underwent fluoroscopically guided bipolar pacing-lead insertion into the RA appendage connected to a pacemaker in the neck. After 24 hours of postoperative recovery, dogs were paced at 600 bpm to maintain fibrillatory atrial activity. For the terminal study, dogs were anesthetized with morphine (2 mg/kg subcutaneously) and α-chloralose (120 mg/kg intravenous bolus, followed by 29.25 mg/kg per hour maintenance dose) and ventilated mechanically. Control animals were anesthetized with sodium pentobarbital (30 mg/kg), intubated and mechanically ventilated. Hearts were removed after right thoracotomy and heparin injection. In the present study, canine tissue was used for antibody validation only; these tissues had been obtained during previous experiments and fast-frozen in liquid nitrogen for subsequent use.

Western blot analyses

Human atrial whole-tissue lysates, human cardiomyocyte fractions, HL-1 cells, dog atrial cardiomyocytes, or dog atrial fibroblasts were subjected to electrophoresis on 5%, 10%, 12% or 15% acrylamide gels, followed by transfer onto polyvinyl difluoride (PVDF) membranes. Protein levels were quantified by Western blotting using the primary antibodies listed in **Online Table V**.[25] The Ser2808-RyR2 and Ser2814-RyR2 phospho-epitope-specific antibodies were custom generated using the peptide C-RTRRI-(pS)-QTSQV corresponding to the protein kinase A (PKA)-dependent phosphorylation site region at Ser2808 and peptide CSQTSQV-(pS)-VD corresponding to the Ca^{2+}/calmodulin-dependent protein kinase-II (CaMKII)-dependent phosphorylation site region at Ser2814, as previously described.[10,11] Appropriate near-infrared fluorophore dyes (IRDye, all 1:15,000 or 1:20,000, LI-COR Biosciences, Lincoln, NE) were employed as secondary antibodies and imaged with an Odyssey Infrared Imaging System (LI-COR Biosciences). Protein expression was normalized to GAPDH or to total protein-levels at 250 kDa (Ponceau staining). Samples excluded from Western blot analyses due to technical issues or because patients did not meet the inclusion criteria for this study have been indicated in the complete Western blot overview available online.

Online Table V. Antibodies used for Western blot experiments.

Target	Antibody (Manufacturer)	Dilution	Host
ASC	sc-22514-R (Santa Cruz) and sc-514414 (Santa Cruz)	1:500	Rabbit / Mouse
α-SMA	A5228 (Sigma-Aldrich)	1:500	Mouse
Calmodulin	ab45689 (Abcam)	1:1,000	Rabbit
Calsequestrin2	PA1-913 (Thermo Fisher)	1:2,500	Rabbit
CaMKIIδ (Total)	611293 (BD Biosciences)	1:1,000	Mouse
CaMKIIδ (Thr287)	ab32678 (Abcam)	1:1,000	Mouse
(Pro-)Caspase-1	sc-56036 (Santa Cruz) and 3019-100 (Biovision)	1:250	Mouse / Rabbit
Caspase-1 (p20)	AG-20B-0042-C100 (AdipoGen)	1:500	Mouse
CD68	ab201973 (Abcam)	1:200	Mouse
CD206	ab64693 (Abcam)	1:500	Rabbit
Collagen1a1	sc-25974 (Santa Cruz)	1:200	Goat
Connexin40	AB1726 (Merck Millipore)	1:500	Rabbit
Connexin43	3511 (Cell Signaling)	1:200	Rabbit
F4/80	ab16911 (Abcam)	1:500	Rat
Fibronectin	sc-8422 (Santa Cruz)	1:1,000	Mouse
GAPDH	5G4 6C5 (HyTest)	1:20,000	Mouse
Gasdermin-D	PA5-30823 (Thermo Fisher) and G7422 (Sigma-Aldrich)	1:500	Rabbit
(Pro-)IL-1β	ab9722 (Abcam)	1:250	Rabbit
MMP9	ab38898 (Abcam)	1:200	Rabbit
cMyBP-C	ab133499 (Abcam)	1:1,000	Rabbit
NCX1	R3F1 (Swant)	1:1,000	Goat
NFκB (Total)	NB100-56712 (Novus Biologicals)	1:500	Mouse
NFκB (Ser536)	NB100-82088 (Novus Biologicals)	1:500	Rabbit
NLRP3	NBP1-77080 (Novus Biologicals)	1:500	Rabbit
P2X7R	sc-15200 (Santa Cruz)	1:250	Goat
PLB (Total)	ab2865 (Abcam)	1:2,000	Mouse
PLB (Ser16)	ab92697 (Abcam)	1:1,000	Rabbit
PLB (Thr17)	A010-13 (Badrilla)	1:2,500	Rabbit
RyR2 (Total)	MA3-916 (Thermo Fisher)	1:1,000	Mouse
RyR2 (Ser2808)	Custom	1:1,000	Rabbit
RyR2 (Ser2814)	Custom	1:2,000	Rabbit
SERCA2a	sc-8095 (Santa Cruz)	1:2,000	Goat
TGF-β1	ab9758 (Abcam)	1:200	Rabbit
TLR4	NB100-56566 (Novus Biologicals)	1:250	Mouse
Troponin-C	10R-T122a (Fitzgerald)	1:500	Mouse
Troponin-I	4002 (Cell Signaling)	1:500	Rabbit
Vimentin	sc-373717 (Santa Cruz)	1:1,000	Mouse

RyR2 single-channel recordings

Single-channel recordings of the cardiac ryanodine receptor type-2 (RyR2) channel were obtained as previously described.[10,11,27] In brief, atrial SR membrane-preparations were incorporated into lipid-bilayer membranes comprising a 3:1 mixture of phosphatidylethanolamine and phosphatidylserine (Avanti Polar Lipids, Alabaster, AL) dissolved in n-decane (25-mg/mL). Bilayers were formed across a 150-μm aperture of a polystyrene cuvette, with the *cis* and *trans* chambers corresponding to the cytosolic and luminal sides of the SR, respectively. The *trans* chamber contained (in mmol/L): HEPES 250, KCl 50 and $Ca(OH)_2$ 53. The *cis* chamber contained (in mmol/L): HEPES 250, Tris-base 125, KCl 50, EGTA 1, and $CaCl_2$ 0.5 (pH=7.35), resulting in 150-nmol/L free cytosolic [Ca^{2+}] (as

determined using MaxChelator, http://maxchelator.stanford.edu/). Ryanodine (5-µmol/L) was applied to the *cis* chamber at the end of each experiment to confirm identity of RyR2 channels. Data were collected using Digidata 1322A (Molecular Devices, Sunnyvale, CA) and Warner Bilayer Clamp Amplifier BC-535 (Warner Instruments, Hamden, CT) under voltage-clamp conditions at 0 mV. Data were analyzed from digitized current recordings using pCLAMP-9.2 software (Molecular Devices) and open probability, as well as mean open and closed times were determined.

Computational Modeling

Baseline (Ctl) model

Our recent model of human atrial cardiomyocyte Ca^{2+}-handling[15] was used as the basis for all simulations. The current model consists of 101 longitudinal segments of 1-µm, each containing 18 1-µm wide transverse domains. In each of these spatial units, local ion concentrations, including cytosolic and SR $[Ca^{2+}]$ are simulated. RyR2 were incorporated in a banded pattern with RyR2 in every other segment, resulting in a 2-µm distance between RyR2 bands, in line with experimental observations.[28] We employed homogeneous expression of RyR2 within a band. Stochastic opening of individual RyR2 was simulated using a 4-state Markov model that reproduces single-channel recordings, as previously described.[11] All RyR2 gate independently, but are connected through a local subspace (the SR Ca^{2+}-release space; SRS), representing the microdomain in the vicinity of the RyR2 with high local $[Ca^{2+}]$ during systole.

Parameter optimization was performed to minimize the quantitative differences between the Ctl model and the experimentally observed Ca^{2+}-handling properties using the published values as starting point. These optimizations in Ca^{2+} diffusion, SERCA, NCX and RyR2 (**Online Table VI**) allowed the model to quantitatively reproduce all major Ca^{2+}-handling properties observed under voltage-clamp conditions (RyR2 open probability, CaT amplitude and decay, SR Ca^{2+} content and SERCA activity; **Online Figures XV-XVII**). Finally, the extracellular Ca^{2+} dependence of NCX was adjusted to prevent excessive Ca^{2+} overload during simulations with 5-mmol/L extracellular $[Ca^{2+}]$ and maximal conductance of two ion channels (I_{K1} and I_{NaK}) were adjusted based on experimental data obtained under current clamp conditions (**Online Table VI**).

The full model code (implemented in C++ with an optional interface to Octave/Matlab for data analysis) is available on the authors' website (http://www.jordiheijman.net).

POAF model variant

We developed a new POAF model variant by incorporating the major differences in Ca^{2+} handling between Ctl and POAF patients: higher SERCA activity and RyR2 open probability. In particular, maximal SERCA2a activity ($J_{SERCA,max}$) was increased by 30%, and RyR2 open probability was increased by adjusting $P[0]_{RyR}$ (+37.7%) and $P[5]_{RyR}$ (+348%), in line with our simulations of higher RyR2 open probability in paroxysmal AF.[11] Finally, the interaction between RyR2 was adjusted by lowering the diffusion of Ca^{2+} from the SRS to the cytosol ($\tau_{diff,SRS \leftrightarrow cyt}$, -16.67%) in order to maintain normal SR Ca^{2+} release in the presence of altered RyR2 gating. With the changes in these 4 parameters (**Online Table VI**, grey rows), the model accurately reproduced the higher SERCA activity and RyR2 open probability (**Online Figure XVA** and **Online Figure XVIE**). Moreover, simulated diastolic and systolic $[Ca^{2+}]$, CaT amplitude, time constant of CaT decay and SR Ca^{2+} load (**Online Figure XVI**), as well as relative SR Ca^{2+} leak (**Online Figure XVII**) in the POAF model variant were quantitatively similar to our experimental data, further establishing the validity of this novel model variant.

Simulating experimental protocols

Extracelullar ionic concentrations and voltage-clamp protocols were set to match experimental conditions for each simulation. During ruptured-patch voltage-clamp simulations, intracellular Na^+ levels were clamped to 8.5-mmol/L as previously described.[11] The effects of tetracaine and caffeine on RyR2 were simulated by acutely setting RyR2 open probability to 1.0 (in the case of caffeine) or blocking RyR2 by >99% (in the case of tetracaine). After the application of tetracaine or caffeine, RyR2 gating was released and open probability was again determined by cytosolic and SR $[Ca^{2+}]$.

Experimental data on the acute effects of (post-operative) inflammation on cardiomyocyte Ca^{2+}-handling are scarce, particularly for human atrial cardiomyocytes. Accordingly, we opted for a parsimonious approach with a minimal number of parameter changes to simulate IL-1β application. Reduced CaT amplitude is a highly consistent finding in response to acute (5 min – 24 hours) stimulation with IL-1β, IL-6 or tumor necrosis factor-α (TNFα).[30,64-67] In several (but not all[67]) studies the reduced CaT amplitude is accompanied by a reduced SR Ca^{2+} content and increased incidence of SCaEs.[30,65] Furthermore, conflicting evidence exists about SERCA function, with reports of both unchanged[67] and decreased[65,68] SERCA2a expression, as well as decreased expression of the SERCA2a-inhibitory subunit phospholamban,[68] which could potentially normalize SERCA function in the presence of decreased expression. Similarly, both unchanged[64] and reduced[65] $I_{Ca,L}$ in response to IL-1β, IL-6 or tumor necrosis factor-α (TNF) stimulation have been reported. Taking into account differences in inflammatory factors and stimulus durations, these data suggest increased RyR2-mediated SR Ca^{2+} leak as a potential mechanism underlying reduced CaT amplitude and increased incidence of SCaEs. Accordingly, we simulated IL-1β stimulation as an additional 25% increase in RyR2 open probability (**Online Figure XV**) and altered diffusion of Ca^{2+} between the SRS units and from the SRS to the cytosol ($\tau_{diff,SRS \leftrightarrow cyt}$; **Online Table VI**), reflecting the coupling between neighboring RyR2. With this minimal set of changes in 3 parameters, the model could quantitatively reproduce the experimentally observed difference in SCaE incidence between Ctl and POAF during acute stimulation with 40-ng/mL IL-1β (**Online Figure XVIII**). Since the effects of IL-1β application are associated with a slight delay due to the activation of the intracellular signaling cascades that eventually lead to alterations in Ca^{2+}-handling proteins, the parameter changes were implemented gradually over a period of 10 seconds.

Online Table VI. Changes in model parameters compared to the reference model of the human atrial cardiomyocyte with spatial Ca^{2+} handling.[15]

	Parameter	Published model[15]	Ctl (+IL-1β) model	poAF (+IL-1β) model
Ca^{2+}-diffusion and buffering	$\tau_{diff,SRS \leftrightarrow cyt}$ (ms)	10	12 (**7.5**)	10
	$\tau_{diff,seg,SRS}$ (ms)	0.220	0.150	0.150 (**0.100**)
	$\tau_{diff,dom,SRS}$ (ms)	0.160	0.050	0.050 (**0.040**)
	Ca^{2+}-buffer factor	1.000	0.850	0.850
SERCA	$J_{SERCA,max}$ (mmol/L ms^{-1})	3.187e-3	2.124e-3	2.762e-3
	SERCA2a $K_{m,r}$ (mmol/L)	1.250	1.750	1.750
	SERCA2a $K_{m,f}$ (mmol/L)	6.250e-4	5.000e-4	5.000e-4
NCX	$I_{NCX,max}$ (pA/pF)	4.253	1.842	1.842
	$[Ca^{2+}]_o$ observed (mmol/L)	1.0*$[Ca^{2+}]_o$	0.1*$[Ca^{2+}]_o$	0.1*$[Ca^{2+}]_o$
RyR2	N_{RyRs}	2,772,000	9,900,000	9,900,000
	$P[0]_{RyR}$	0.200	0.620	0.85374
	$P[5]_{RyR}$	0.0035	0.0147 (**0.018375**)	0.06581 (**0.08226**)
	$P[7]_{RyR}$	9.000e-4	1.000e-3	1.000e-3
	$P[8]_{RyR}$	8.000e-5	7.000e-5	7.000e-5
Other ion channels	$G_{K1,max}$ (mS/µF)	6.563e-2	9.188e-2	9.188e-2
	$I_{NaK,max}$ (pA/pF)	1.260	0.630	0.630
	I_{CaL}		Ctl and POAF as in Voigt et al.[6] with $ACT_\infty = \frac{1}{\left(1+exp\left(-\frac{V_M-13.56}{7.0}\right)\right)} \cdot \frac{1}{\left(1+exp\left(-\frac{V_M+25}{5.0}\right)\right)}$	

Grey shaded rows highlight parameters that are different between Ctl and POAF model version. Bold numbers in orange represent parameter values during simulated IL-1β stimulation.

Supplemental Analyses

Online Table VII. Overview of statistical properties and tests employed. Intra-class correlation coefficient (ICC) for experiments in which one patient can provide multiple data points, normality of data distribution for Ctl and POAF groups or HL-1 cells in the absence or presence of IL-1β assessed using the D'Agostino & Pearson omnibus normality test, statistical test employed to compare both groups based on these characteristics and corresponding P-values for all parameters studied. Significant values are shown in bold.

Fig.	Parameter	ICC	Norm. dist. (Ctl / POAF)	Statistical Test	P-value
1B	$I_{Ca,L}$ amplitude (ruptured patch)	<0.01	Yes / No	Multilevel models with log-transformed data	0.425
1C	CaT amplitude	0.107	Yes / Yes	Multilevel models	**0.007**
1D	τ CaT decay	0.252	No / Yes	Multilevel models with log-transformed data	0.121
2B	cCaT amplitude	0.302	Yes / Yes	Multilevel models	0.638
2B	SR Ca^{2+} load / Integrated I_{NCX}	0.501	Yes / Yes	Multilevel models	0.675
2C	Peak caffeine-induced I_{NCX}	0.394	Yes / No	Multilevel models with log-transformed data	0.580
2C	Slope I_{NCX} vs. $[Ca^{2+}]_i$	0.460	No / No	Multilevel models with log-transformed data	0.902
2D	k_{syst}	0.212	Yes / Yes	Multilevel models	0.135
2D	k_{caff}	0.944	Yes / Yes	Multilevel models	0.921
2D	k_{SERCA}	<0.01	Yes / Yes	Multilevel models	0.075
3A	SR Ca^{2+} leak/load (Na^+/Ca^{2+}-free)	<0.01	Yes / No	Multilevel models with log-transformed data	**0.035**
3C	SCaE incidence (Na^+/Ca^{2+}-free)	0.037	No / Yes	Multilevel models with log-transformed data	**0.011**
3E	Spontaneous I_{NCX} incidence at -50 mV (perforated patch)	0.878	No / No	Multilevel models with log-transformed data	**0.044**
4A	RyR2 Open probability	0.260	Yes / No	Multilevel models with log-transformed data	**0.009**
4A	RyR2 Mean open time	0.173	No / No	Multilevel models with log-transformed data	0.561
4A	RyR2 Mean closed time	<0.01	Yes / No	Multilevel models with log-transformed data	**0.046**
4C	Total-RyR2	N/A	Yes / Yes	Unpaired Student's *t*-test	0.884
4C	Ser2814-RyR2	N/A	Yes / Yes	Unpaired Student's *t*-test	0.323
4C	Ser2814/Total-RyR2	N/A	Yes / Yes	Unpaired Student's *t*-test	**0.040**
4C	Total-CaMKIIδ$_C$	N/A	Yes / Yes	Unpaired Student's *t*-test	**0.019**
4C	Thr287-CaMKIIδ$_C$	N/A	Yes / Yes	Unpaired Student's *t*-test with Welch's correction	**0.021**
4C	Thr287/Total-CaMKIIδ$_C$	N/A	Yes / Yes	Unpaired Student's *t*-test	0.166
5A	NLRP3 (125 kDa)	N/A	Yes / Yes	Unpaired Student's *t*-test with Welch's correction	**0.023**
5A	ASC	N/A	Yes / Yes	Unpaired Student's *t*-test with Welch's correction	0.056
5A	Pro-Casp1	N/A	Yes / Yes	Unpaired Student's *t*-test with Welch's correction	**0.038**
5A	GSDMD-FL	N/A	N/D / N/D	Mann-Whitney test	**0.030**
5A	Pro-IL-1β	N/A	Yes / Yes	Unpaired Student's *t*-test	0.178

5A	Casp1-p20	N/A	N/D / N/D	Mann-Whitney test	0.413
5A	GSDMD-NT	N/A	N/D / N/D	Mann-Whitney test	0.931
5A	IL-1β	N/A	Yes / Yes	Unpaired Student's *t*-test with Welch's correction	0.402
5B	TLR4	N/A	Yes / Yes	Unpaired Student's *t*-test with Welch's correction	**0.032**
5B	NFκB-total	N/A	Yes / Yes	Unpaired Student's *t*-test with Welch's correction	**0.027**
5B	NFκB-Ser536	N/A	Yes / No	Mann-Whitney test	0.468
5B	NFκB-Ser536/Total-NFκB	N/A	Yes / Yes	Unpaired Student's *t*-test	0.426
5B	P2X7R	N/A	Yes / Yes	Unpaired Student's *t*-test with Welch's correction	**0.008**
5C	F4/80	N/A	Yes / Yes	Unpaired Student's *t*-test	**0.019**
5C	CD68	N/A	Yes / Yes	Unpaired Student's *t*-test with Welch's correction	**0.035**
5C	CD206	N/A	Yes / Yes	Unpaired Student's *t*-test	0.416
6F	NLRP3 (125 kDa)	N/A	Yes / Yes	Unpaired Student's *t*-test with Welch's correction	0.534
6F	ASC	N/A	Yes / Yes	Unpaired Student's *t*-test with Welch's correction	**0.004**
6F	Pro-Casp1	N/A	Yes / No	Mann-Whitney test	**0.006**
6F	GSDMD-FL	N/A	Yes / Yes	Unpaired Student's *t*-test with Welch's correction	**0.041**
6F	Pro-IL-1β	N/A	Yes / Yes	Unpaired Student's *t*-test with Welch's correction	**0.029**
6G	Casp1-p37	N/A	Yes / No	Mann-Whitney test	**<0.001**
6G	Casp1-p20	N/A	Yes / No	Mann-Whitney test	0.174
6G	Casp1-p10	N/A	Yes / Yes	Unpaired Student's *t*-test with Welch's correction	**0.002**
6G	GSDMD-NT	N/A	Yes / Yes	Unpaired Student's *t*-test with Welch's correction	**0.008**
6G	GSDMD-CT	N/A	Yes / Yes	Unpaired Student's *t*-test	**0.015**
6G	IL-1β	N/A	Yes / No	Mann-Whitney test	0.054
7C	Susceptibility to SCaEs	N/A	Categorical	Fisher's exact test	**0.003**
7D	SCaE incidence (5 mmol/L Ca^{2+} + IL-1β)	<0.01	No / Yes	Multilevel models with log-transformed data	**0.003**
Fig.	**Parameter**	**ICC**	**Norm. dist. (-IL-1β / +IL-1β)**	**Statistical Test**	**P-value**
8A	SCaE incidence HL-1 cells (5 mmol/L Ca^{2+} + IL-1β)	N/A	Yes / Yes	Unpaired Student's *t*-test	**0.031**
8C	Ser2808-RyR2	N/A	Yes / Yes	Unpaired Student's *t*-test with Welch's correction	**0.023**
8C	Ser2814-RyR2	N/A	Yes / Yes	Unpaired Student's *t*-test with Welch's correction	**0.001**
8C	Ser16-PLB	N/A	Yes / Yes	Unpaired Student's *t*-test	0.115
8C	Thr17-PLB	N/A	Yes / Yes	Unpaired Student's *t*-test with Welch's correction	**0.004**
8D	Ser2808-RyR2 KN-92/KN-93	N/A	Yes / Yes	Unpaired Student's *t*-test	0.239
8D	Ser2814-RyR2 KN-92/KN-93	N/A	Yes / Yes	Unpaired Student's *t*-test	**<0.001**
8D	Ser16-PLB KN-92/KN-93	N/A	Yes / Yes	Unpaired Student's *t*-test	0.457

8D	Thr17-PLB KN-92/KN-93	N/A	Yes / Yes	Unpaired Student's *t*-test with Welch's correction	**0.002**
8F	NLRP3 (125 kDa)	N/A	Yes / Yes	Unpaired Student's *t*-test	0.264
8F	Pro-Caspase1	N/A	Yes / Yes	Unpaired Student's *t*-test	0.229
8F	GSDMD-FL	N/A	Yes / Yes	Unpaired Student's *t*-test	0.318
8F	Casp1-p20	N/A	Yes / Yes	Unpaired Student's *t*-test with Welch's correction	**0.011**
8F	GSDMD-NT	N/A	Yes / Yes	Unpaired Student's *t*-test	**0.027**
8G	Casp1-p20 KN-92/KN-93	N/A	Yes / Yes	Unpaired Student's *t*-test	0.123
8G	GSDMD-NT KN-92/KN-93	N/A	No / No	Mann-Whitney test	0.762
Fig.	**Parameter**	**ICC**	**Norm. dist. (Ctl / POAF)**	**Statistical Test**	**P-value**
IIA	$I_{Ca,L}$ integral (ruptured patch)	0.451	No / Yes	Multilevel models with log-transformed data	0.435
IIB	Diastolic $[Ca^{2+}]_i$	0.258	No / Yes	Multilevel models with log-transformed data	0.982
IIB	Systolic $[Ca^{2+}]_i$	0.191	Yes / Yes	Multilevel models	0.246
IIC	CaT time to peak	0.660	No / No	Multilevel models with log-transformed data	0.121
IIIA	$I_{Ca,L}$ amplitude (perforated patch)	<0.01	No / No	Multilevel models with log-transformed data	0.580
IIIC	V_{mid} $I_{Ca,L}$ inactivation (perforated patch)	0.268	No / No	Multilevel models with log-transformed data	0.159
IIID	τ_{fast} $I_{Ca,L}$ inactivation (perforated patch)	0.709	Yes / No	Multilevel models with log-transformed data	0.133
IIID	τ_{slow} $I_{Ca,L}$ inactivation (perforated patch)	<0.01	No / Yes	Multilevel models with log-transformed data	**<0.001**
IIIF	τ $I_{Ca,L}$ recovery (perforated patch)	<0.01	Yes / Yes	Multilevel models	**0.007**
IVB	Prevalence of alternans (perforated patch)	N/A	Categorical	Chi-squared	**0.005**
IVC	Frequency of beat-to-beat variability (perforated patch)	0.137	No / Yes	Multilevel models with log-transformed data	0.459
VB	RMP	N/A	Yes / Yes	Unpaired Student's *t*-test	0.346
VB	dVdtmax	N/A	Yes / Yes	Unpaired Student's *t*-test	0.622
VB	Conduction time	N/A	Yes / Yes	Unpaired Student's *t*-test	0.169
VB	APD20	N/A	No / No	Mann-Whitney test	0.846
VB	APD50	N/A	Yes / Yes	Unpaired Student's *t*-test	0.815
VB	APD90	N/A	Yes / Yes	Unpaired Student's *t*-test	0.245
VIA	Integrated I_{NCX} (perforated patch)	0.106	Yes / Yes	Multilevel models	0.675
VIB	Spontaneous I_{NCX} incidence at -80 mV (perforated patch)	0.255	No / No	Multilevel models with log-transformed data	0.999
VII	SERCA	N/A	Yes / Yes	Unpaired Student's *t*-test	0.657
VII	Total-PLB	N/A	Yes / Yes	Unpaired Student's *t*-test	0.604
VII	Ser16-PLB	N/A	Yes / Yes	Unpaired Student's *t*-test	**0.047**
VII	Ser16-PLB/Total-PLB	N/A	Yes / Yes	Unpaired Student's *t*-test	0.120
VII	Thr17-PLB	N/A	Yes / No	Mann-Whitney test	0.487
VII	Thr17-PLB/Total-PLB	N/A	Yes / No	Mann-Whitney test	0.651
VII	NCX1 (160 kDa)	N/A	Yes / Yes	Unpaired Student's *t*-test	0.620
VII	NCX1 (120 kDa)	N/A	No / Yes	Mann-Whitney test	0.888
VIIA	SR Ca^{2+} leak	0.126	Yes / Yes	Multilevel models	0.090

	(Na^+/Ca^{2+}-free)				
VIIB	cCaT amplitude (Na^+/Ca^{2+}-free)	<0.01	Yes / Yes	Multilevel models	**0.030**
VIIC	SR Ca^{2+} leak/load (Na^+/Ca^{2+}-free)	<0.01	Yes / No	Multilevel models with log-transformed data	**0.035**
VIIID	cMyBP-C	N/A	Yes / Yes	Unpaired Student's *t*-test	0.172
VIIID	Troponin-C	N/A	Yes / Yes	Unpaired Student's *t*-test with Welch's correction	0.291
VIIID	Troponin-I	N/A	Yes / Yes	Unpaired Student's *t*-test	0.071
VIIID	Calmodulin	N/A	Yes / Yes	Unpaired Student's *t*-test	0.950
IXA	Total-RyR2 (from Ser2808)	N/A	Yes / Yes	Unpaired Student's *t*-test with Welch's correction	0.482
IXA	Ser2808-RyR2	N/A	Yes / Yes	Unpaired Student's *t*-test	0.680
IXA	Ser2808/Total-RyR2	N/A	Yes / Yes	Unpaired Student's *t*-test	0.261
IXB	Calsequestrin	N/A	No / Yes	Mann-Whitney test	0.881
X	Total-CaMKIIδ_B+δ_9	N/A	Yes / Yes	Unpaired Student's *t*-test	0.239
X	Thr287-CaMKIIδ_B+δ_9	N/A	Yes / Yes	Unpaired Student's *t*-test	0.102
X	Thr287/Total-CaMKIIδ_B+δ_9	N/A	Yes / Yes	Unpaired Student's *t*-test	0.176
XIII	Fibronectin	N/A	Yes / No	Mann-Whitney test	0.671
XIII	Col1a1	N/A	Yes / Yes	Unpaired Student's *t*-test	0.194
XIII	Vimentin	N/A	Yes / Yes	Unpaired Student's *t*-test	0.424
XIII	MMP9	N/A	Yes / Yes	Unpaired Student's *t*-test	0.336
XIII	α-SMA	N/A	Yes / No	Mann-Whitney test	0.081
XIII	TGF-β1	N/A	Yes / Yes	Unpaired Student's *t*-test	0.230
XIV	Total-Cx40	N/A	Yes / Yes	Unpaired Student's *t*-test	0.214
XIV	Total-Cx43	N/A	Yes / No	Mann-Whitney test	0.281
XIV	Ser368-Cx43	N/A	Yes / No	Mann-Whitney test	0.094
XIV	Ser368/Total-Cx43	N/A	No / No	Mann-Whitney test	0.536
	Multiple (Fig. XXII – XXXII)	N/A	N/A	Two-way ANOVA	Mult.
XXIXA	Severity of mitral valve insufficiency	N/A	Categorical	Chi-squared	0.160
XXXA	Severity of tricuspid valve insufficiency	N/A	Categorical	Chi-squared	0.525
XXXIA	Severity of aortic valve insufficiency	N/A	Categorical	Chi-squared	0.836
XXXIIIA	NLRP3 (125 kDa) original analysis	N/A	Yes / Yes	Unpaired Student's *t*-test with Welch's correction	**0.023**
XXXIIIB	NLRP3 (125 kDa) blinded re-analysis	N/A	Yes / Yes	Unpaired Student's *t*-test with Welch's correction	**0.016**

Online Table VIII. Overview of P-values for two-way ANOVA analyses with factors post-operative rhythm (Ctl vs. POAF) and either age (<73 vs. ≥73 years), sex (male vs. female), left-atrial diameter (LAD; <42 vs. ≥42 mm), degree of mitral valve insufficiency (MVI, none/mild vs. moderate/severe), tricuspid valve insufficiency (TVI, none vs. mild/moderate) or aortic valve insufficiency (AVI, none vs. mild/moderate/severe), or beta-blockers (BBs) or statin use (no vs. yes) for expression levels of NLRP3-inflammasome components and Ca^{2+}-handling parameters. P-values <0.05 have been indicated in orange. $^{\$}$ indicates significant (P<0.05) interaction with post-operative rhythm status (i.e., differences associated with the clinical variable are only observed in Ctl or POAF samples). P=N/A indicates the inability to perform two-way ANOVA because there are no patients in one of the four combinations of post-operative rhythm and clinical status. Selected parameters are shown in **Online Figures XXII-XXXII**. Due to the number of comparisons and number of patients in each of the four combinations, the statistical power and robustness of these subanalyses is limited and results should be considered hypothesis generating.

	Clinical Variable							
Parameter	**Age**	**Sex**	**LAD**	**MVI**	**TVI**	**AVI**	**BBs**	**Statins**
NLRP3	P=0.994	P=0.265	P=0.817	P=0.923	P=0.922	P=0.737	P=0.846	P=0.015
ASC	P=0.322	P=0.820	P=0.703	P=0.580	P=0.844	P=0.554	P=0.080	P=0.416
Pro-Caspase1	P=0.976	P=0.462	P=0.791	P=N/A	P=0.808	P=0.908	P=0.138	P=0.593
GSDMD-FL	P=0.182	P=0.793	P=N/A	P=0.524	P=0.606	P=0.134	P=0.898	P=N/A
Pro-IL-1β	P=0.411	P=0.196	P=0.339	P=0.104	P=0.272	P=0.862	P=0.638	P=0.579
IL-1β	P=0.870	P=0.594	P=0.338	P=0.550	P=0.123	P=0.646	P=0.372	P=0.974
TLR4	P=0.047	P=0.914	P=0.658	P=N/A	P=0.390	P=0.434	P=0.907	P=0.646
NFκB-Total	P=0.130	P=0.864	P=0.739	P=0.577	P=0.524	P=0.100	P=0.045	P=0.086
P2X7R	P=0.220	P=0.782	P=0.642	P=0.091	P=0.426	P=0.996	P=0.774	P=0.334
CD68	P=0.983	P=0.618	P=0.002	P=0.893	P=0.365	P=0.048$^{\$}$	P=0.178	P=0.276
Fibronectin	P=0.142	P=0.458	P=0.186	P=0.958	P=0.051	P=0.006$^{\$}$	P=0.868	P=0.295
CaMKIIδ_C-Total	P=0.340	P=0.129	P=N/A	P=0.915	P=0.904	P=0.363	P=0.394	P=0.105
CaMKIIδ_C-Thr287	P=0.035	P=0.397	P=N/A	P=0.179	P=0.985	P=0.469	P=0.031	P=0.752
PLB-Total	P=0.802	P=0.058	P=0.116	P=0.322	P=0.856	P=0.326	P=0.483	P=0.581
PLB-Ser16	P=0.535	P=0.183	P=0.458	P=0.450	P=0.992	P=0.014	P=0.666	P=0.462
PLB-Thr17	P=0.887	P=0.365	P=0.205	P=0.009$^{\$}$	P=0.866	P=0.017	P=0.452	P=0.016
RyR2-Total	P=0.490	P=0.300	P=0.206	P=0.266	P=0.194	P=0.909	P=0.938	P=0.309
RyR2-Ser2814	P=0.222	P=0.256	P=0.505	P=0.144	P=0.720	P=0.212	P=0.239	P=0.399
NCX1 (160 kDa)	P=0.688	P=N/A	P=0.049	P=0.143	P=0.444	P=0.079	P=0.800	P=N/A
C_m	P=0.820	P=0.625	P=0.042	P=0.989	P=0.011	P=0.043	P=0.773	P=0.002
$I_{Ca,L}$ amplitude	P=0.115	P=0.532	P=0.933	P=0.070	P=0.882	P=0.877	P=0.140	P=0.278
CaT amplitude	P=0.736	P=0.256	P=0.204	P=0.225	P=0.142	P=0.096	P=0.882	P=0.303
SCaE incidence (0-mmol/L Na^+/Ca^{2+})	P=0.026	P=0.076	P=0.187	P=N/A	P=0.550	P=0.847	P=0.860	P=0.022
SCaE incidence (IL-1β)	P=0.529	P=N/A	P=N/A	P=0.343	P=0.972	P=N/A	P=0.534	P=0.819

$I_{Ca,L}$ amplitude (perforated patch)	P=0.076	P=0.362	P=0.529	P=N/A	P=N/A	P=N/A	P=0.150	P=0.963
SR Ca^{2+} load (perforated patch)	P=0.263	P=0.697	P=0.808	P=N/A	P=N/A	P=N/A	P=0.249	P=0.610
Spontaneous I_{NCX} (-50 mV)	P=0.198	P=0.077	P=0.140	P=N/A	P=N/A	P=N/A	P=0.593	P=0.593
Spontaneous I_{NCX} (-80 mV)	P=0.510	P=0.192	P=0.137	P=N/A	P=N/A	P=N/A	P=0.561	P=0.118

Supplemental Figures

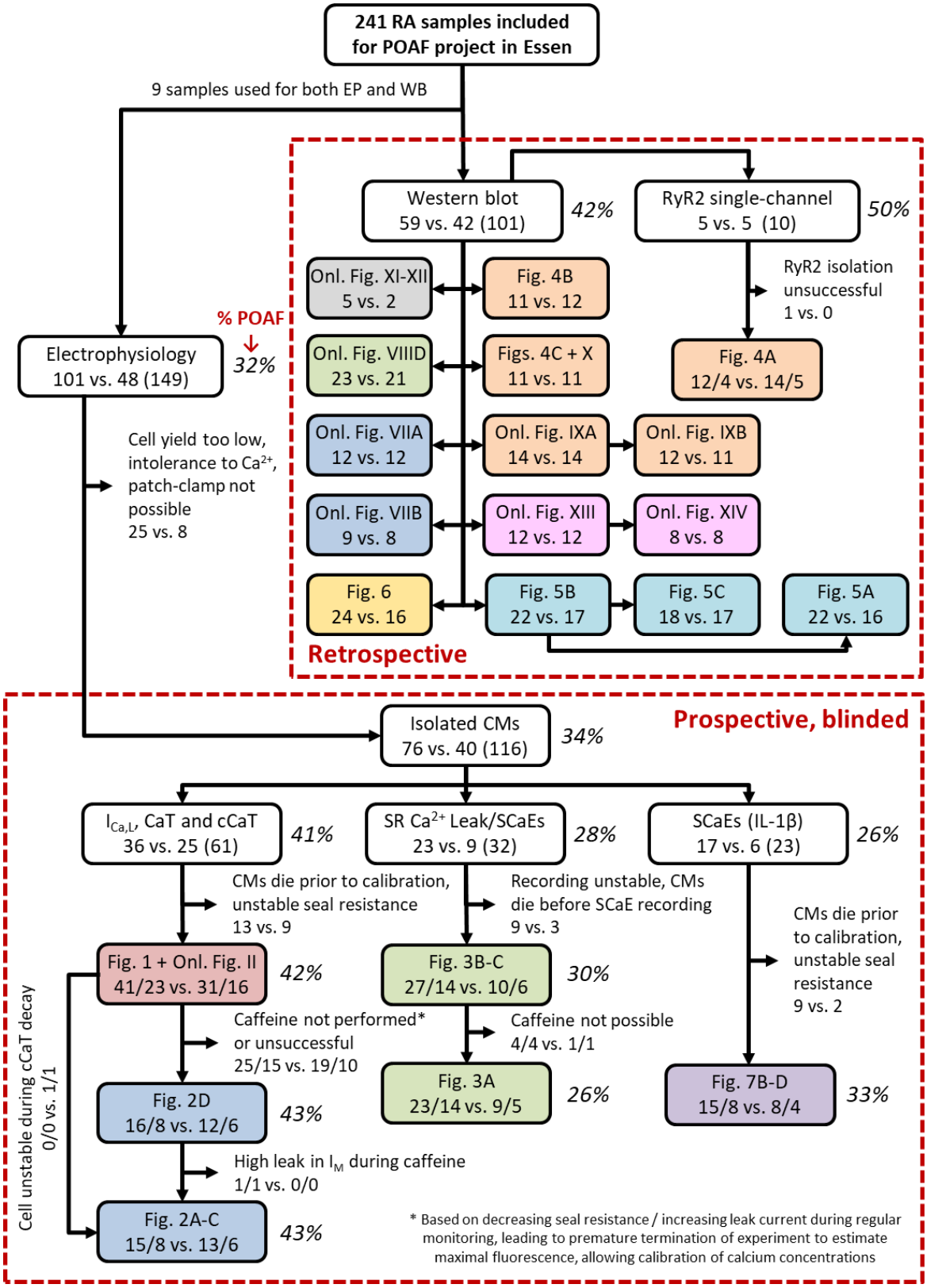

Online Figure I. Flowchart of all samples obtained by the primary research institution from Cardiac Surgery Center Essen Huttrop. Human right-atrial (RA) appendages from Essen were employed for all experiments except for action potential recordings in atrial

trabeculae and validation experiments using the perforated-patch clamp methodology. The number of samples included for individual subsets of experiments is indicated per Figure (Fig.) / Online Figure (Onl. Fig.) and number of unsuccessful experiments and reason for failure is shown. X vs. Y indicates number of Ctl patients vs. number of POAF patients and x/X vs. y/Y indicates number of cardiomyocytes (CMs) / number of patients in both groups. Percentages to the right of individual boxes reflect incidence of POAF. The percentage of patients developing POAF in each series of experiments was of the same order for all “prospective” experiments performed acutely on isolated atrial samples (ranging from 26% through 43%) and did not differ between successful and unsuccessful experiments, making it unlikely that our results were biased because experiments failed more often in one over the other group.

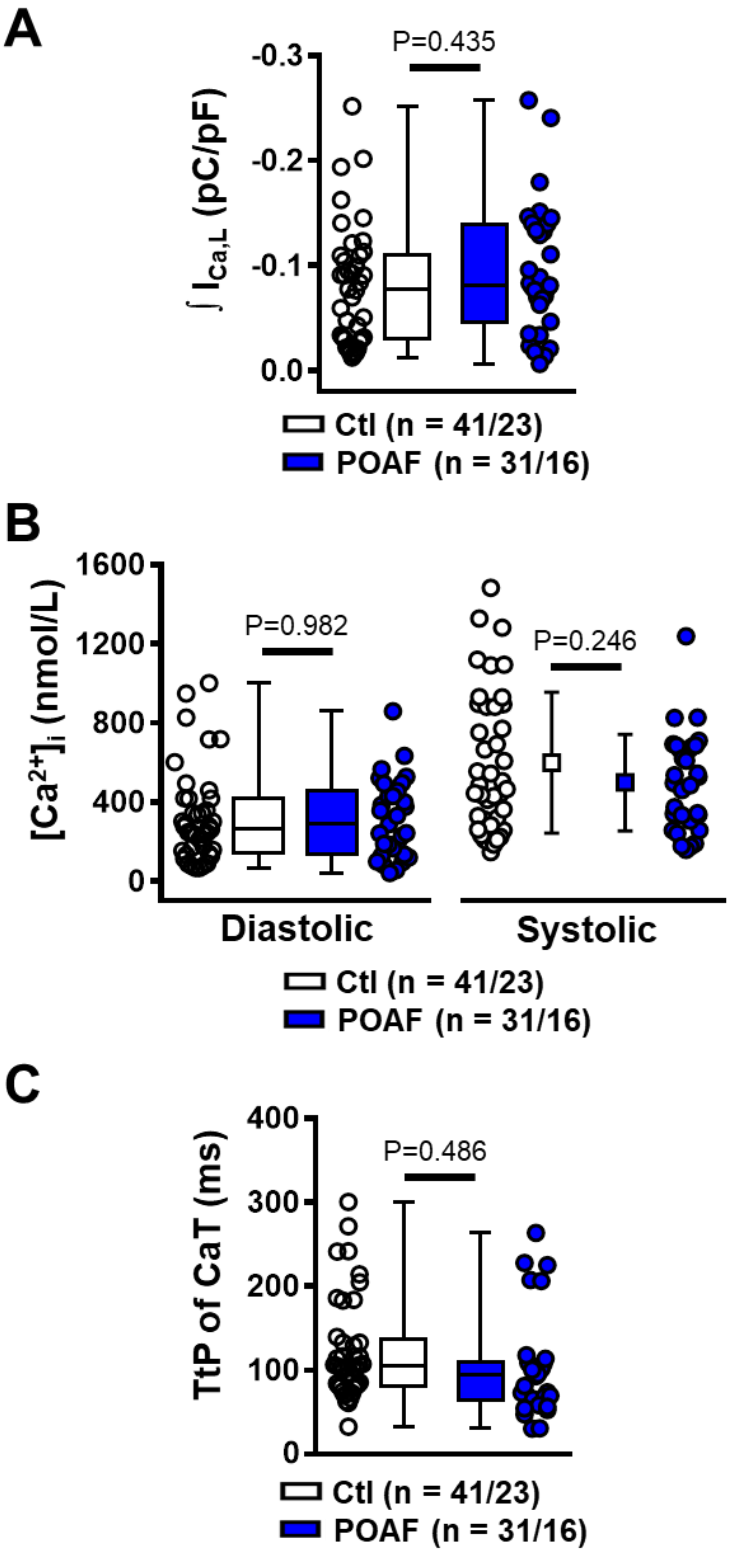

Online Figure II. L-type Ca^{2+} current ($I_{Ca,L}$) and Ca^{2+}-transient (CaT) measured simultaneously during ruptured-patch recordings with Fluo-3 as Ca^{2+} indicator in Ctl and POAF. A, Integrated $I_{Ca,L}$ during a 100-ms depolarizing step to +10 mV. **B-C,** Diastolic and systolic intracellular Ca^{2+} levels (**B**), and time-to-peak (TtP) of the $I_{Ca,L}$-triggered CaT (**C**) in Ctl and POAF. N-numbers indicate numbers of cardiomyocytes/patients. P-values based on multilevel models (systolic Ca^{2+}) or multilevel models with log-transformed data (integrated $I_{Ca,L}$, diastolic Ca^{2+}, TtP).

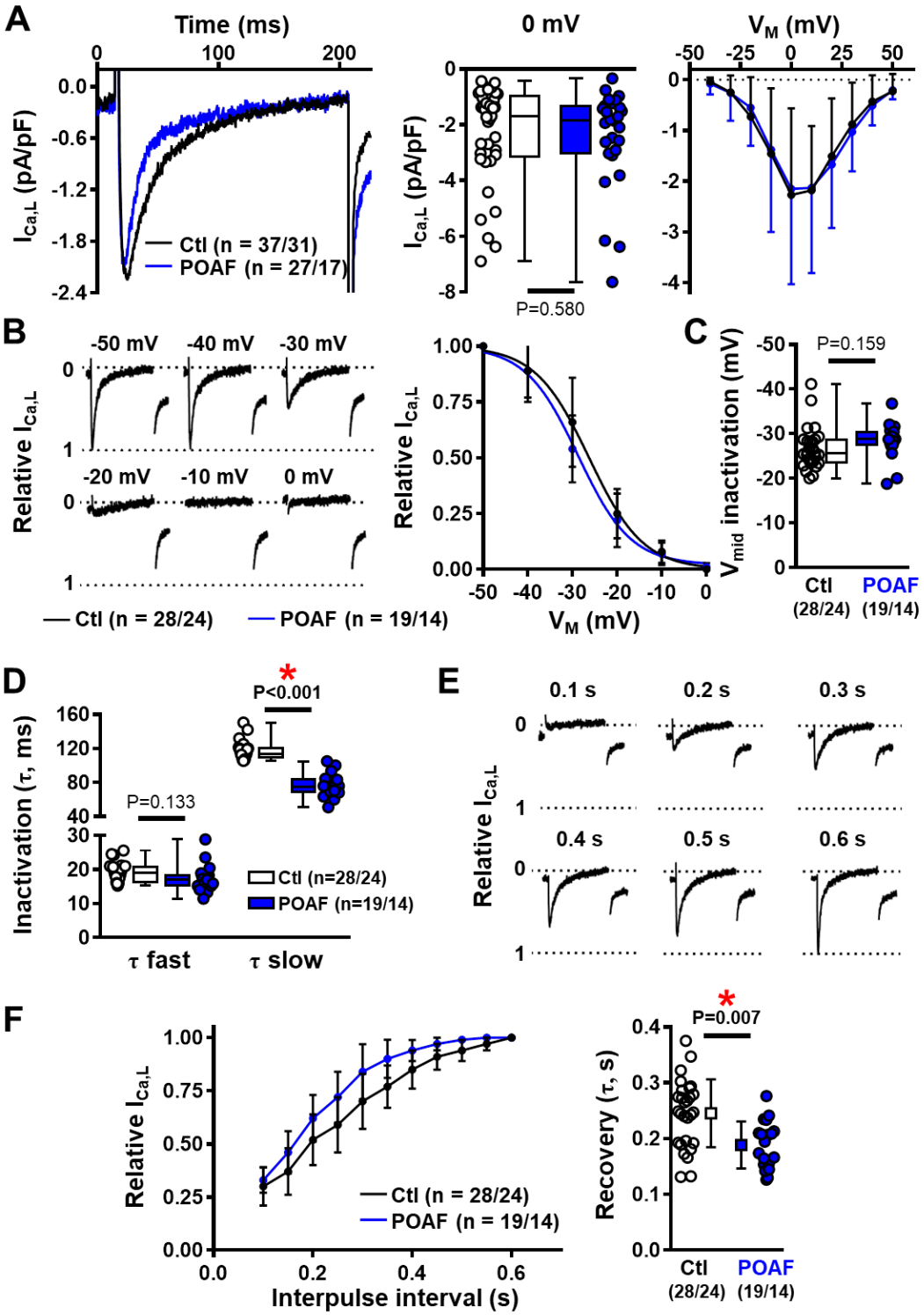

Online Figure III. Properties of the L-type Ca^{2+}-current ($I_{Ca,L}$) during perforated-patch recordings. A, Example of $I_{Ca,L}$ during a 200-ms depolarizing voltage-step to 0 mV in a Ctl and a POAF cardiomyocyte (**left**), group data for $I_{Ca,L}$ amplitude in Ctl and POAF (**middle**), and $I_{Ca,L}$ current-voltage (I-V) relationship (**right**) in Ctl (black symbols / line) and POAF (blue symbols / line) cardiomyocytes. **B,** Examples of $I_{Ca,L}$ inactivation (**left**) and quantification of relative $I_{Ca,L}$ amplitude in Ctl (black line) and POAF (blue line; **right**) analyzed using a test pulse to 0 mV following a 300-ms inactivating pulse to the indicated potential. **C,** Midpoint of inactivation (V_{mid}) obtained using a Boltzmann fit of the individual inactivation I-V curves in Ctl

and POAF cardiomyocytes. **D,** Fast and slow time constants of $I_{Ca,L}$ inactivation obtained using a bi-exponential fit during a 200-ms depolarizing pulse to 0 mV in Ctl and POAF. **E,** Examples of $I_{Ca,L}$ recovery from inactivation assessed using depolarizing pulses to 0 mV for different interpulse intervals at -80 mV. **F,** Quantification of relative $I_{Ca,L}$ amplitude as function of interpulse interval in Ctl and POAF cardiomyocytes (**left**) and time constants of recovery from inactivation assessed using a mono-exponential fit of the individual recovery curves (**right**). N-numbers indicate numbers of cardiomyocytes/patients. **P*<0.05 vs. Ctl based on multilevel models (panel **F**) or multilevel models with log-transformed data (panels **A,C** and **D**).

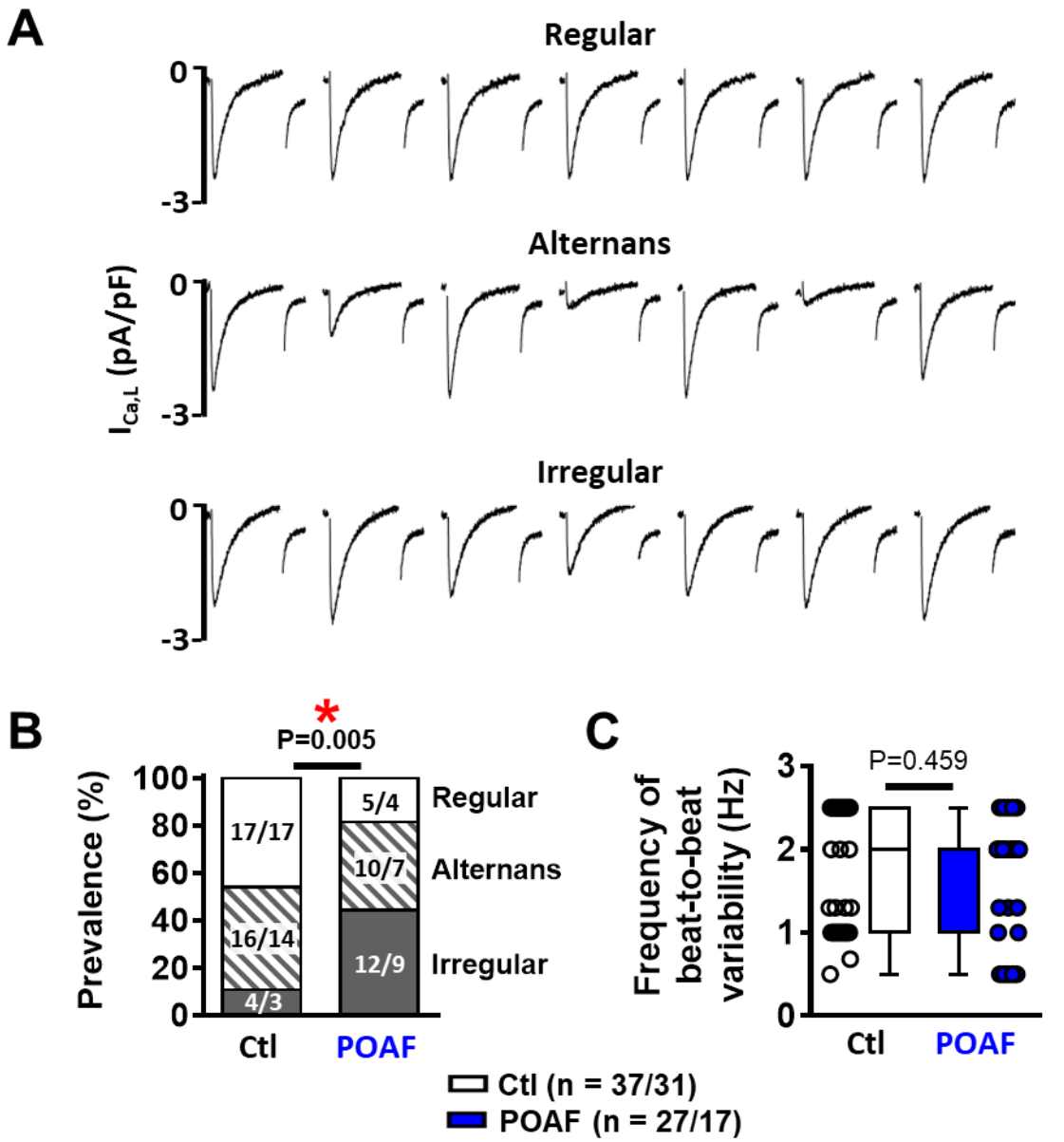

Online Figure IV. L-type Ca^{2+} current ($I_{Ca,L}$) alternans in POAF patients. A, Examples of regular beat-to-beat $I_{Ca,L}$ (**top**), $I_{Ca,L}$ alternans (**middle**) and irregular beat-to-beat $I_{Ca,L}$ alterations (**bottom**) recorded in perforated-patch experiments. **B,** Prevalence of regular, alternans and irregular $I_{Ca,L}$ patterns. **C,** frequency at which beat-to-beat alterations developed (or the maximal frequency of 2.5-Hz if beat-to-beat patterns remained regular) in Ctl and POAF atrial cardiomyocytes. *P<0.05 vs. Ctl based on Chi-squared test (panel **B**) or multilevel models with log-transformed data (panel **C**).

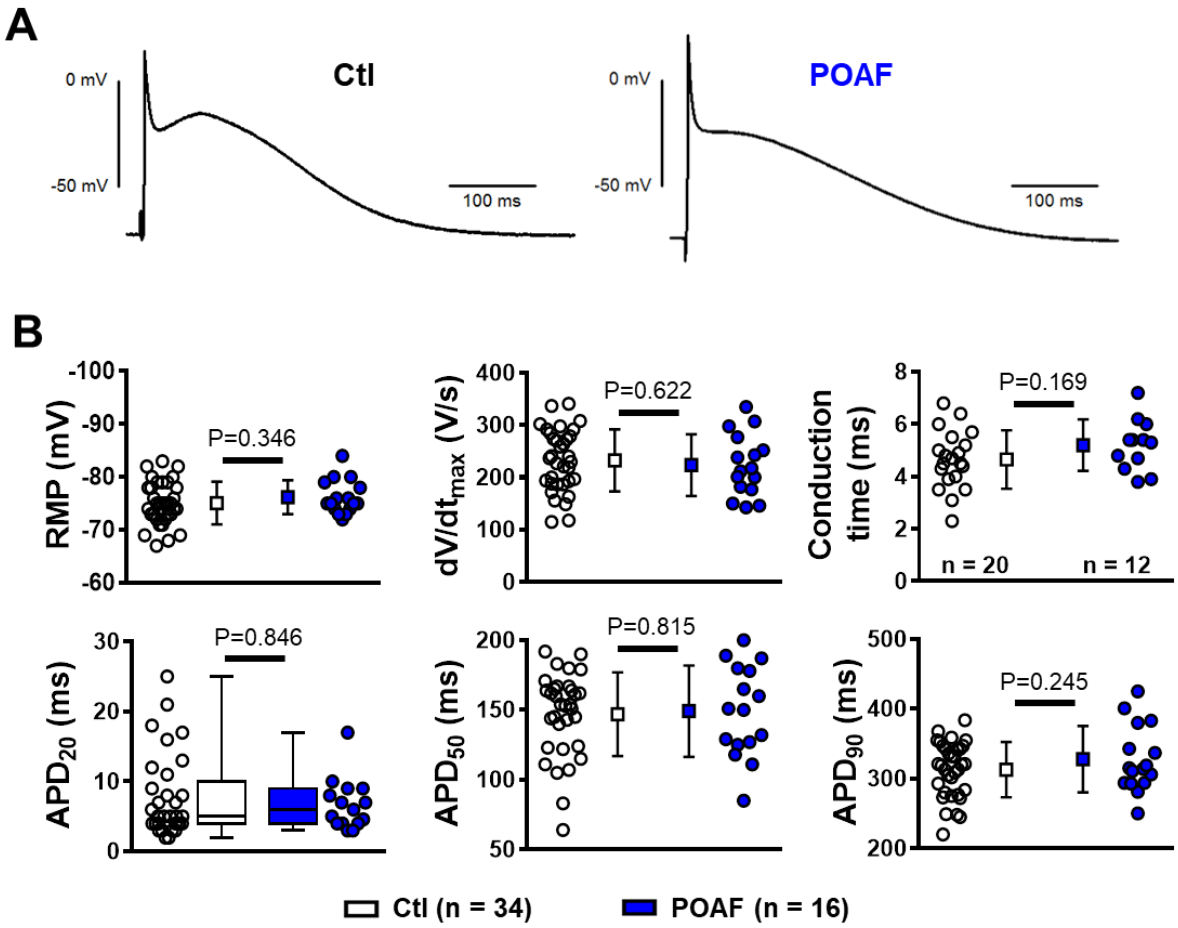

Online Figure V. Electrical remodeling in Ctl and POAF patients. A, Action potentials (APs) at 1-Hz in atrial trabeculae. **B,** Quantification of AP characteristics in Ctl and POAF trabeculae. **Top** row shows resting membrane potential (RMP), maximum upstroke velocity (dV/dt_{max}) and conduction time. **Bottom** row shows AP duration (APD) at 20%, 50% and 90% of repolarization. P-values based on Mann-Whitney test for APD_{20} and unpaired Student's *t*-test for all other parameters.

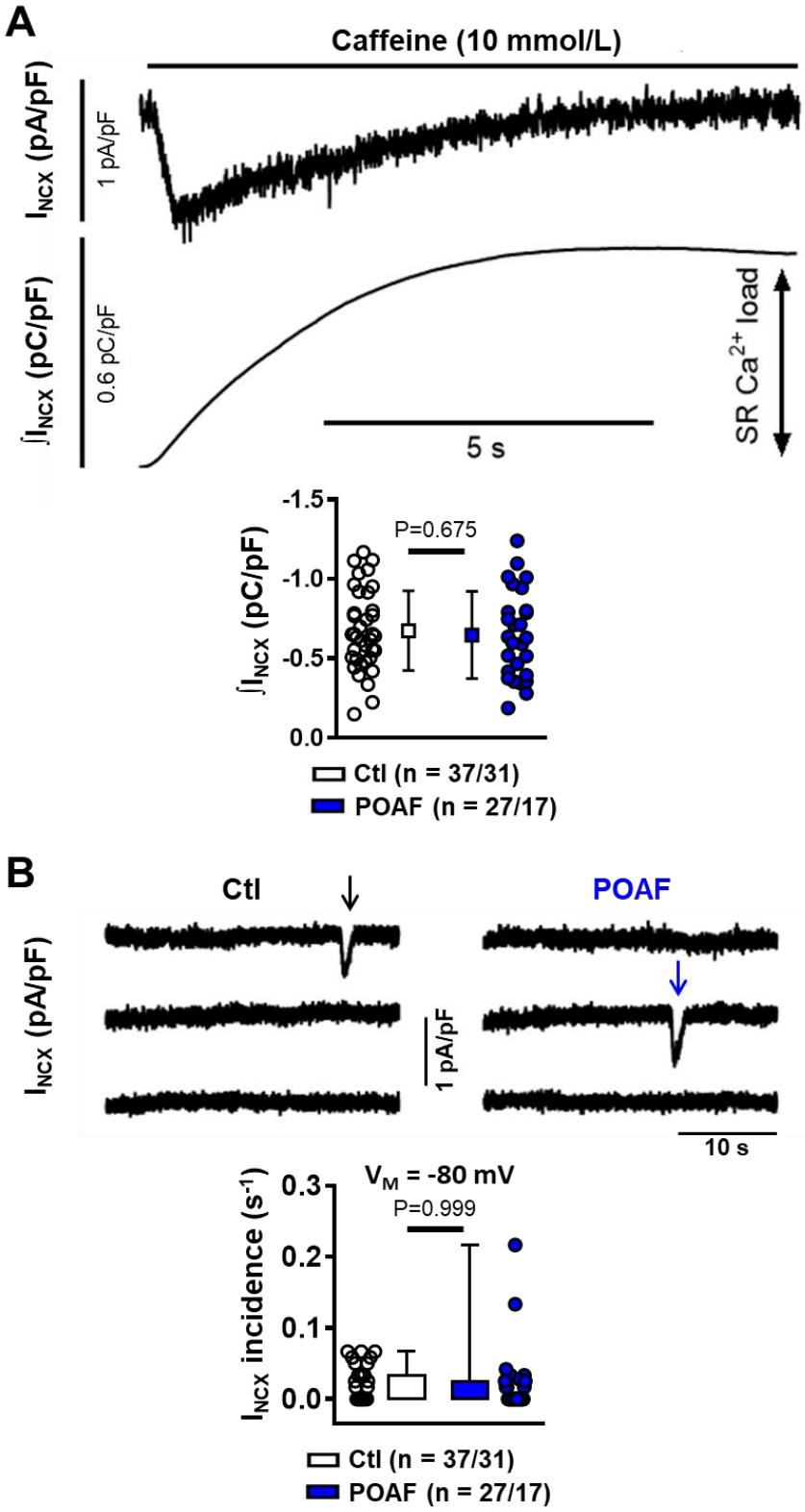

Online Figure VI. Sarcoplasmic reticulum (SR) Ca^{2+} load and spontaneous SR Ca^{2+}-release event-mediated I_{NCX} in perforated-patch experiments. A, Example of absolute and integrated caffeine-induced NCX-mediated inward current (I_{NCX}; **top**) and SR Ca^{2+} load quantified as total integrated I_{NCX} in Ctl and POAF (**bottom**). **B,** Examples of spontaneous I_{NCX} (indicated with arrows) in a Ctl (**left**) and POAF (**right**) cardiomyocyte at a holding potential of -80 mV, and incidence of I_{NCX} in Ctl and POAF cardiomyocytes at a holding potential of -80 mV (**bottom**). P-values based on multilevel models (**A**) or multilevel models with log-transformed data (**B**).

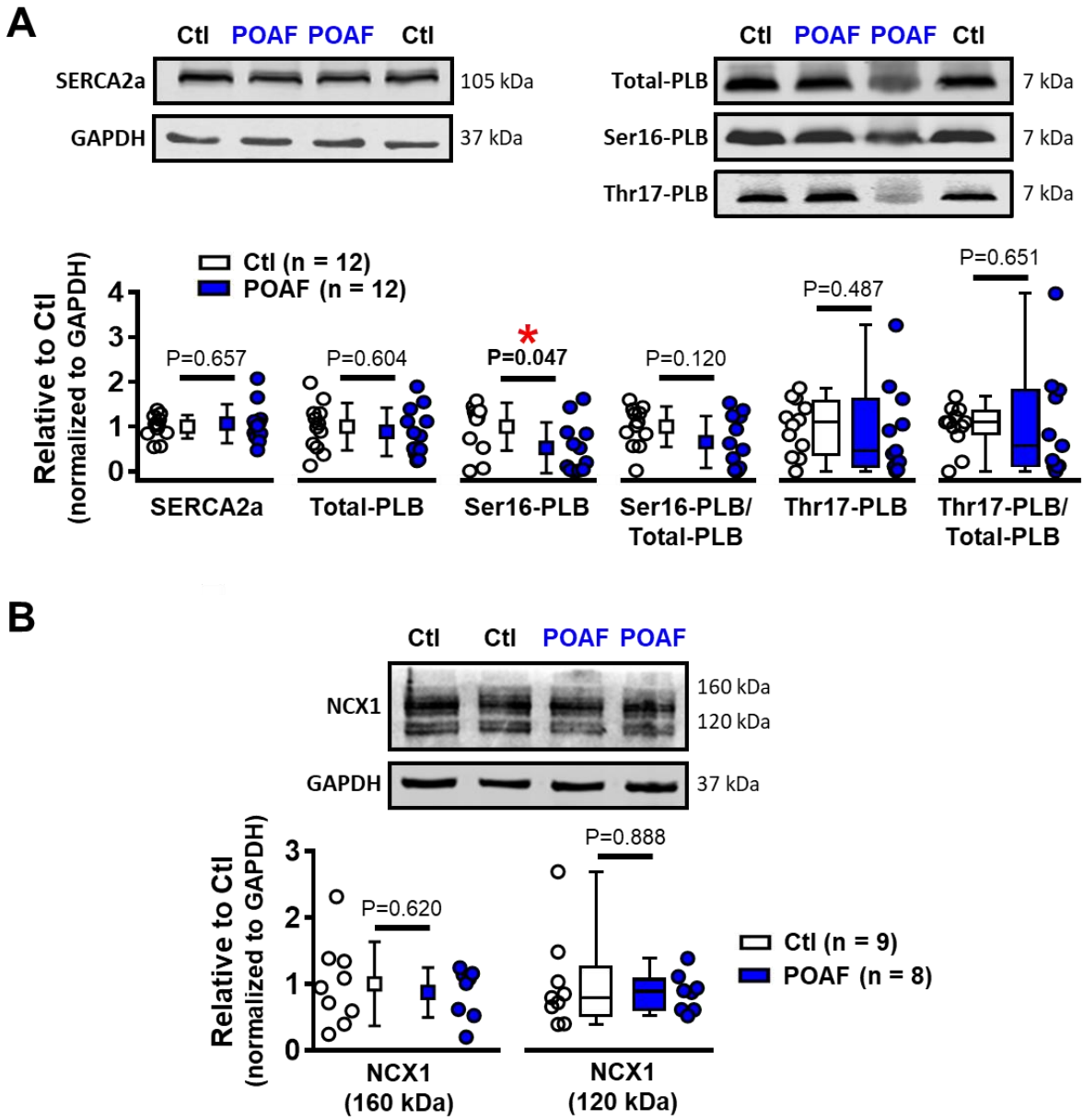

Online Figure VII. Western-blot analysis of the sarcoplasmic reticulum Ca^{2+}-ATPase type-2a (SERCA2a) complex and Na^{+}/Ca^{2+}-exchanger type-1 (NCX1). A, Example Western blots (**top**) and protein levels (**bottom**) of SERCA2a, total, Ser16-phosphorylated and Thr17-phosphorylated phospholamban (PLB) in Ctl and POAF. **B,** Example Western blots (**top**) and protein levels (**bottom**) of full-length (160 kDa) and proteolytic (120 kDa) fragment of NCX1. GAPDH was used as loading control. P-values based on Mann-Whitney test (Thr17-PLB, Thr17-PLB/Total-PLB, and 120 kDa NCX1) or unpaired Student's *t*-test (other proteins).

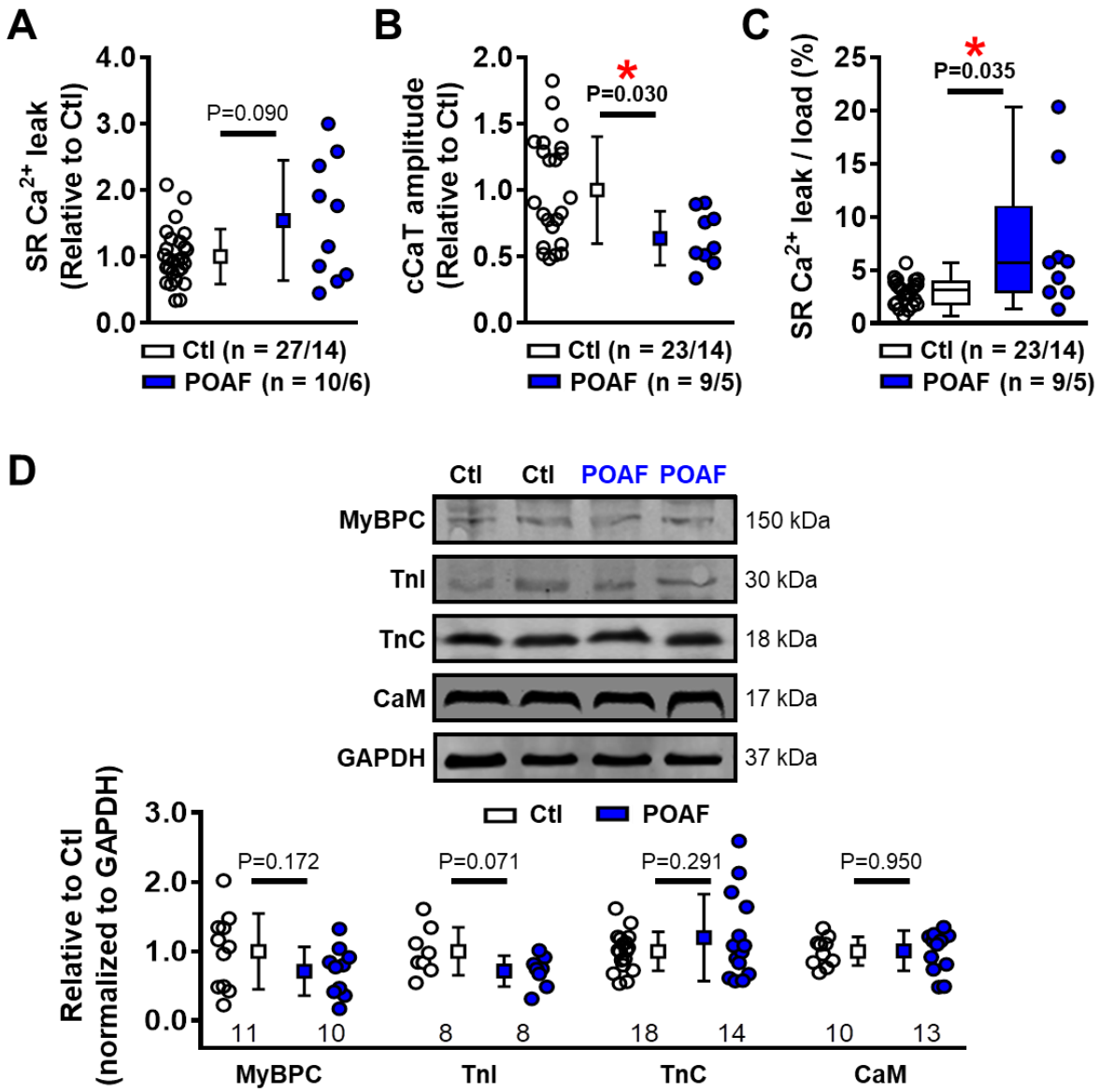

Online Figure VIII. Assessment of sarcoplasmic reticulum (SR) Ca^{2+} leak and Western-blot analysis of major Ca^{2+}-buffering proteins. A, Tetracaine (1-mmol/L)-induced decrease in fluorescence, which is proportional to SR Ca^{2+}-leak, in POAF cardiomyocytes relative to Ctl. **B,** Amplitude of caffeine-induced Ca^{2+}-transient (cCaT), a rough indicator of SR Ca^{2+}-load, in POAF cardiomyocytes relative to Ctl. **C,** SR Ca^{2+}-leak/SR Ca^{2+}-load ratio in Ctl and POAF. **D.** Western blots (**top**) and protein levels (**bottom**) of the major Ca^{2+} buffers cardiac myosin-binding protein-C (MyBPC), cardiac troponin-I (TnI), troponin-C (TnC) and calmodulin (CaM) in human atrial whole-tissue lysates. GAPDH was used as loading control. N-numbers indicate numbers of cardiomyocytes/patients (panels **A-C**) or patients (panel **D**). *P<0.05 vs. Ctl based on multilevel models (**A, B**), multilevel models with log-transformed data (**C**), or unpaired Student's *t*-test (**D**), with Welch's correction for unequal variance for TnC.

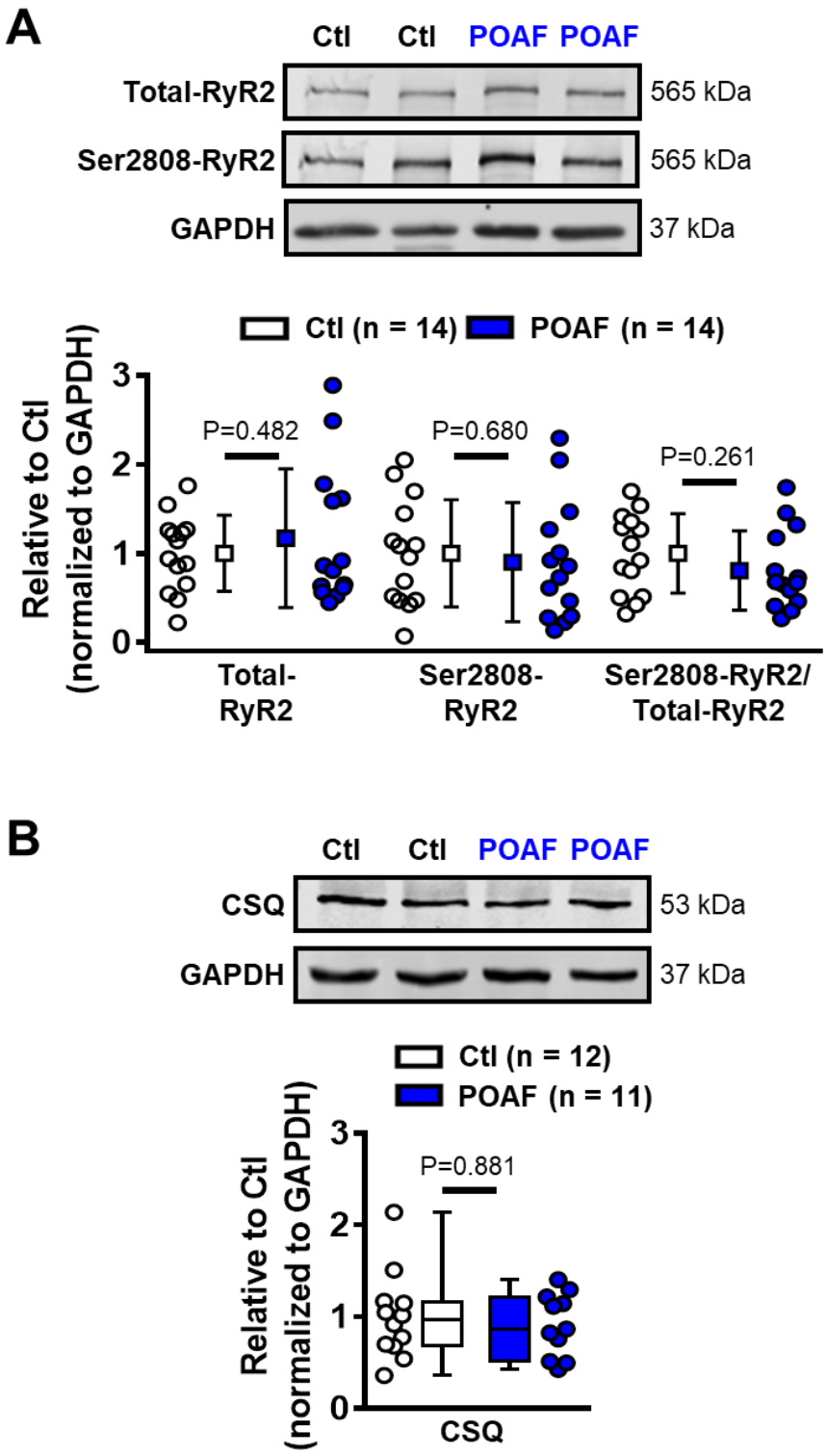

Online Figure IX. Western-blot analysis of ryanodine receptor channel type-2 (RyR2) and calsequestrin (CSQ) regulation in Ctl and POAF patients. A, Example Western blots (**top**) and quantified protein levels (**bottom**) of total and Ser2808-phosphorylated RyR2. **B,** Western blots (**top**) and quantified protein levels (**bottom**) of the sarcoplasmic reticulum (SR) Ca^{2+} buffer and RyR2-regulator CSQ. GAPDH was used as loading control. N-numbers indicate numbers of patients. P-values based on unpaired Student's *t*-test (**A**; with Welch's correction for unequal variance for Total-RyR2) or Mann-Whitney test (**B**).

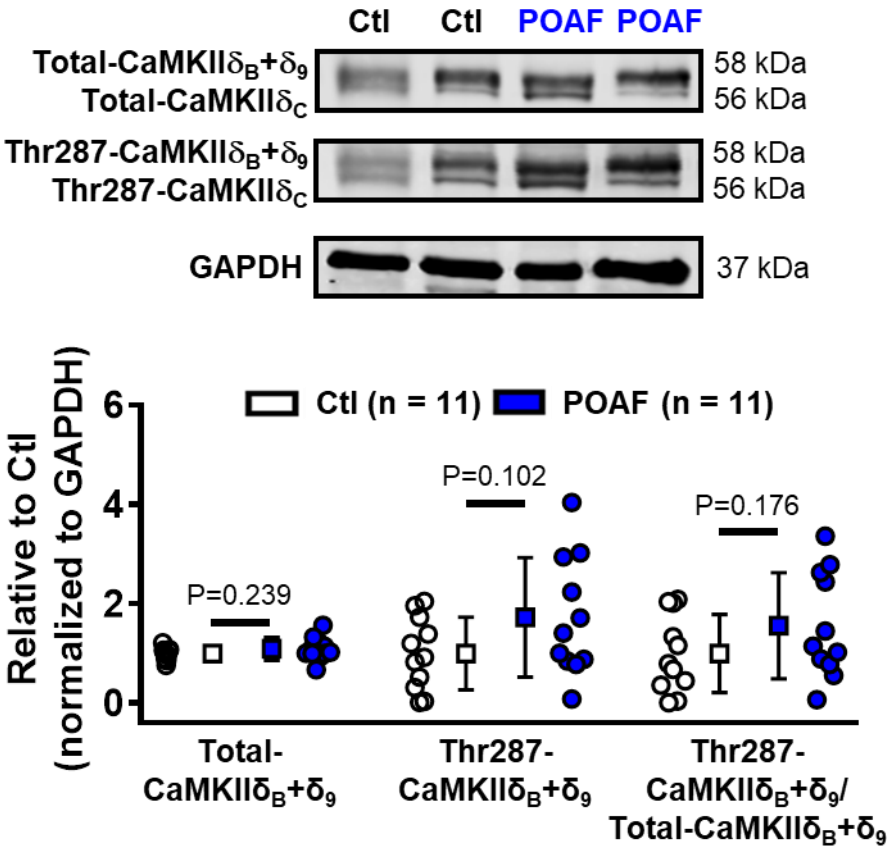

Online Figure X. Western-blot analysis of Ca^{2+}/calmodulin-dependent protein kinase-IIδ (CaMKIIδ) regulation in Ctl and POAF patients. Western blots of total and Thr287-autophosphorylated levels of nuclear and cytosolic CaMKIIδ ($CaMKII\delta_B+\delta_9$ and $CaMKII\delta_C$, respectively; **top**) and quantification of total and Thr287-autophosphorylated $CaMKII\delta_B+\delta_9$ (**bottom**). GAPDH was used as loading control. N-numbers indicate numbers of patients. P-values based on unpaired Student's *t*-test.

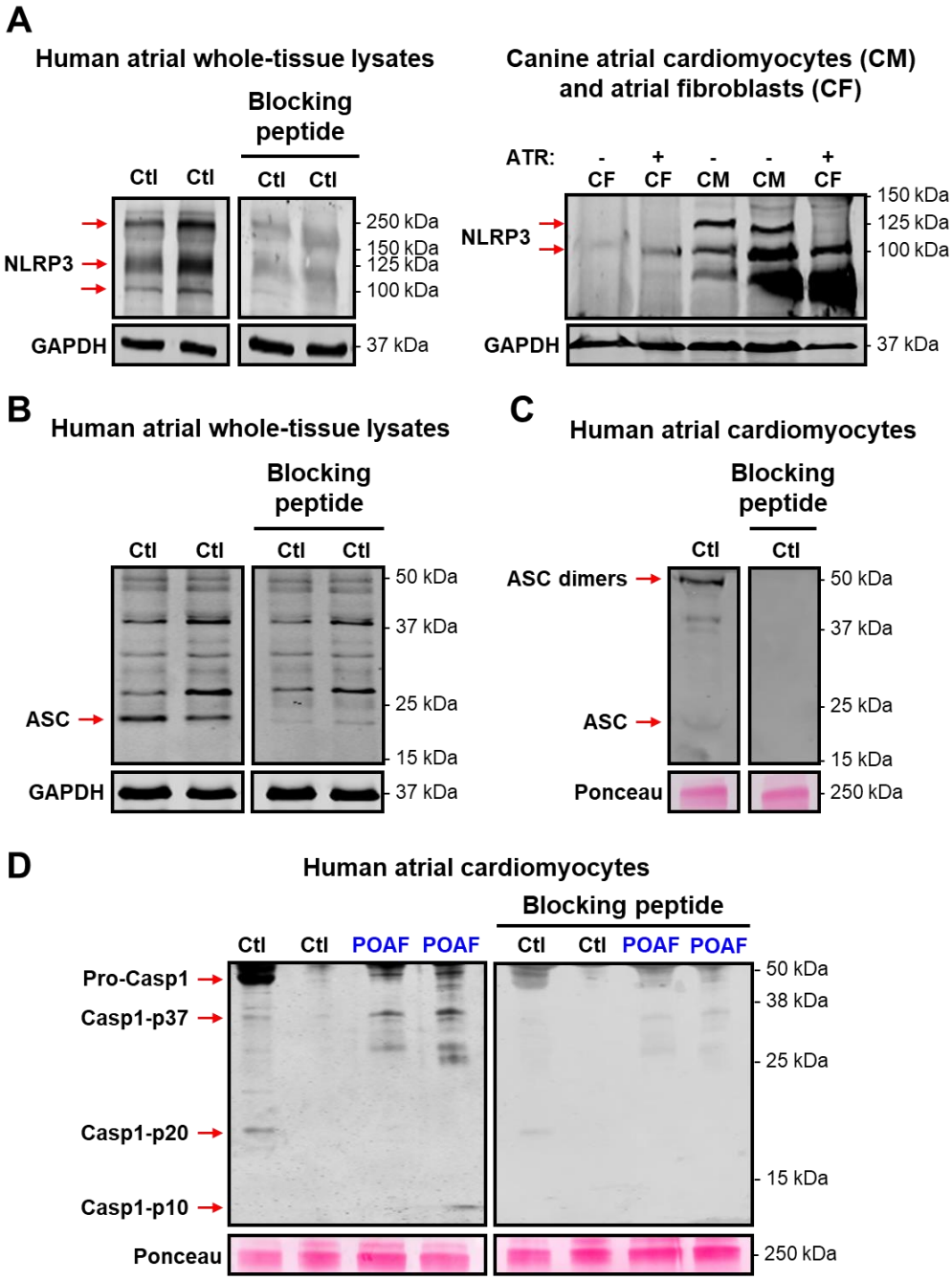

Online Figure XI. Evaluation of antibodies against components of the atrial NACHT, LRR, and PYD domains containing protein 3 (NLRP3) inflammasome used in Western blot experiments. A, Western blots in human atrial whole-tissue lysates of Ctl patients in the absence or presence of blocking peptide (left), as well as in canine atrial cardiomyocyte (CM) or cardiac fibroblast (CF) fractions of dogs with or without atrial tachycardia-related remodeling (ATR, 600 bpm for 2 weeks), identifying specific bands at ~125 kDa (full length) and ~100 kDa (a protein fragment lacking the LRR domain), respectively, as NLRP3.[69] Please note the absence of a ~125 kDa band in dog CFs. **B-C,** Western blots of ASC in the absence or presence of blocking peptide in human atrial whole-tissue lysates (**B**) or human atrial cardiomyocytes (**C**) of Ctl patients, identifying specific bands at ~24 kDa (monomers) and ~48 kDa (dimers), respectively. **D,** Western blots of Pro-caspase-1 (Pro-Casp1) and its cleaved products (Casp1-p37, Casp1-p20, and Casp1-p10) in human atrial cardiomyocytes of Ctl and POAF patients in the absence or presence of blocking peptide, showing specificity of the individual bands. GAPDH or total protein levels at 250 kDa (Ponceau staining) were used as loading control.

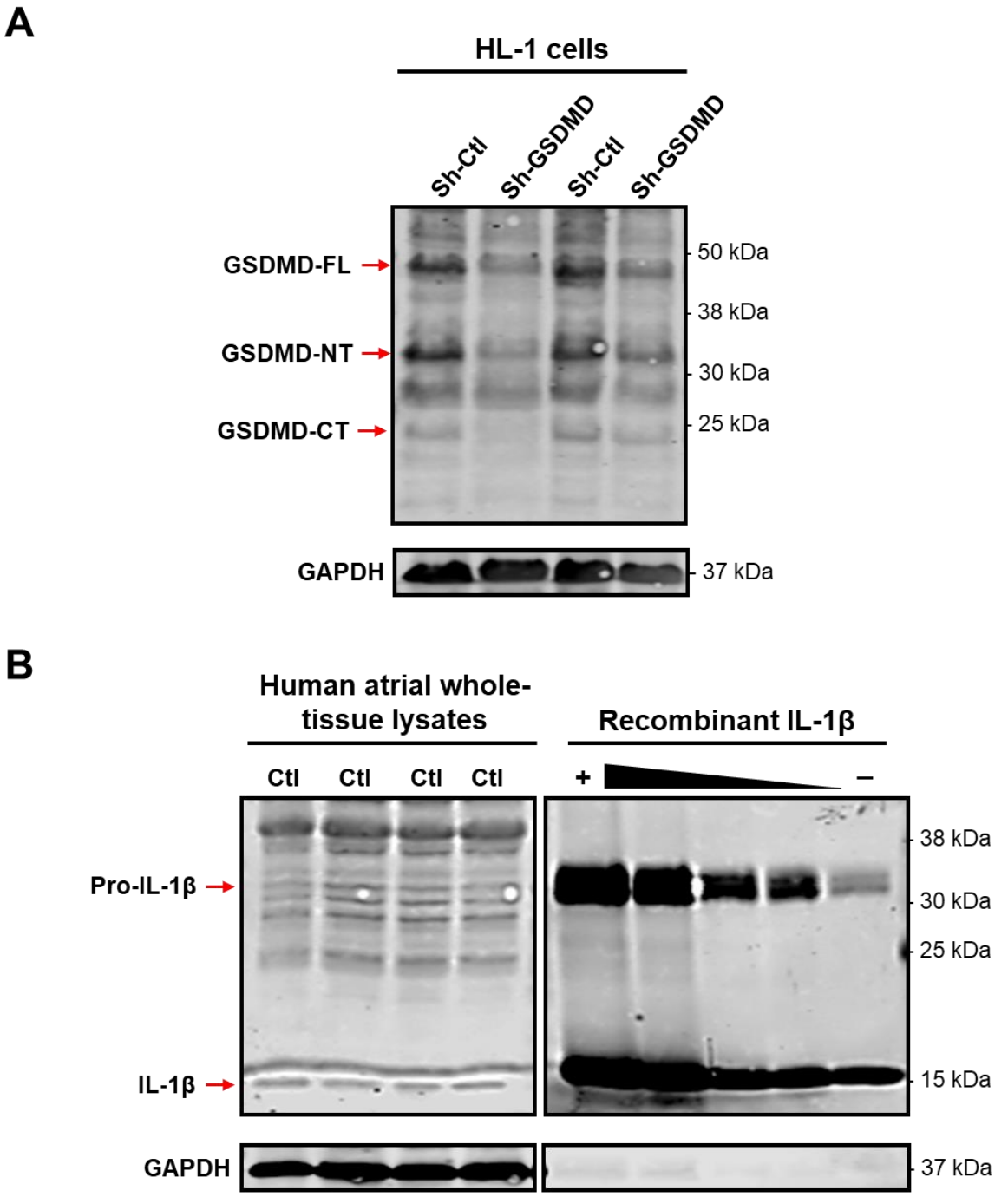

Online Figure XII. Evaluation of antibodies against gasdermin-D (GSDMD) and (Pro-)interleukin-1β (IL-1β) used in Western blot experiments. A, Western blot showing GSDMD full-length (FL), as well as N-terminal (NT) and C-terminal (CT) fragments in HL-1 cells with control short-hairpin (sh) RNA or shRNA-mediated knockdown of GSDMD**.** The 3 GSDMD bands are strongly reduced or abolished with GSDMD knockdown, validating antibody and bands specificity. **B,** Western blots of (Pro-)IL-1β in human atrial whole-tissue lysates of Ctl patients (**left**) compared to different concentrations of recombinant IL-1β (**right**), showing the corresponding IL-1β bands. GAPDH was used as loading control.

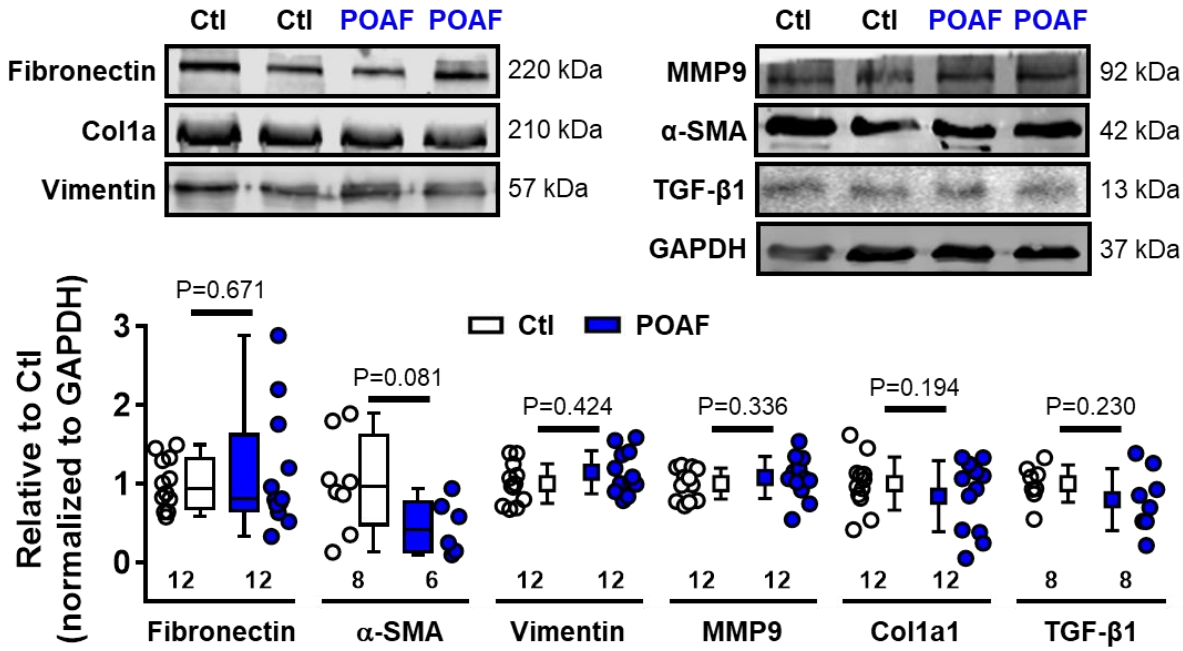

Online Figure XIII. No indices of profibrotic remodeling in POAF patients. Western blots (**top**) and quantified protein levels (**bottom**) of markers of profibrotic remodeling: fibronectin, α-smooth muscle actin (α-SMA), vimentin, collagen 1a1 (Col1a1), matrix metallopeptidase type-9 (MMP9), and transforming growth factor-β1 (TGF-β1). GAPDH was used as loading control. Numbers below symbols indicate number of atrial samples. P-values based on Mann-Whitney test (fibronectin, α-SMA) or unpaired Student's *t*-test (vimentin, MMP9, Col1a1, TGF-β1).

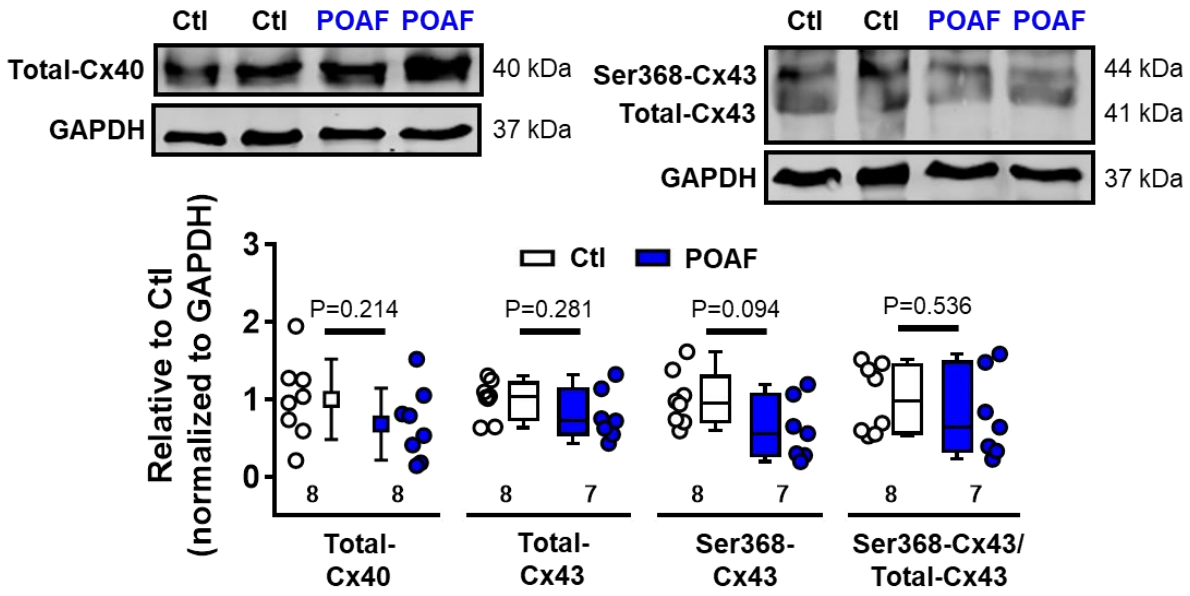

Online Figure XIV. No indices of connexin remodeling in POAF patients. Western blots (**top**) and quantified protein levels (**bottom**) of total connexin-40 (Cx40), as well as total and Ser368-phosphorylated connexin-43 (Cx43). GAPDH was used as loading control. Numbers below symbols indicate number of atrial samples. P-values based on Mann-Whitney test (Total-Cx40) or unpaired Student's *t*-test (Total-Cx43 Ser368-Cx43 and Ser368-Cx43/Total-Cx43).

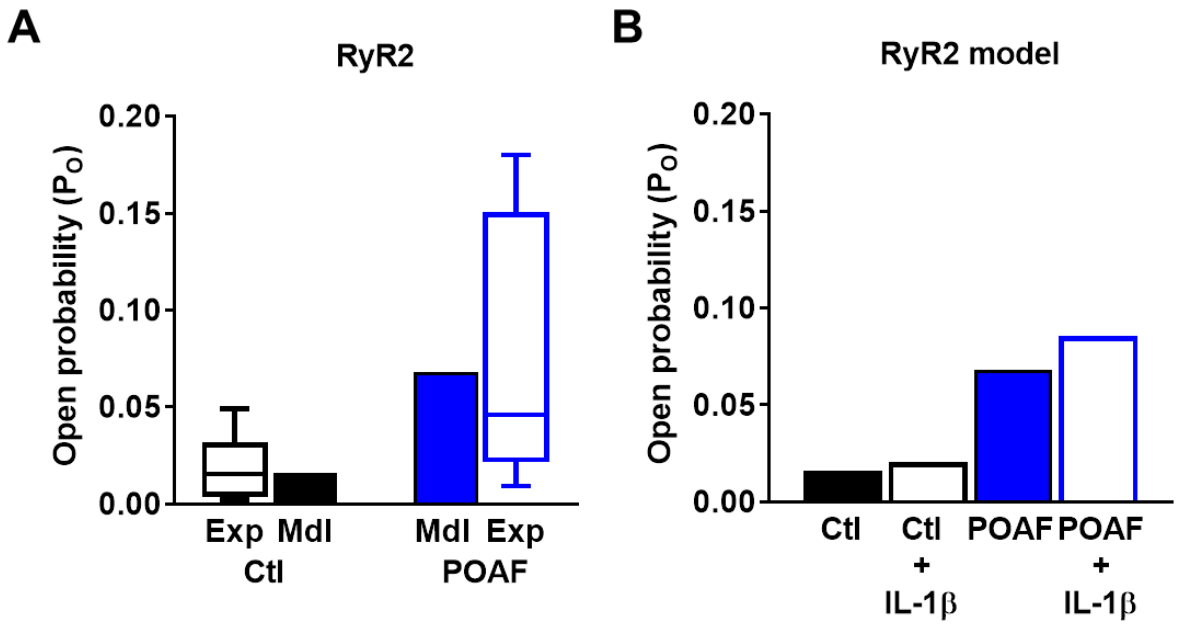

Online Figure XV. Simulated single-channel properties of ryanodine receptor channel type-2 (RyR2) in Ctl and POAF model variants. A, Comparison of simulated RyR2 single-channel open probability in Ctl and POAF models with experimental data from **Figure 4A** under diastole-like conditions (150-nmol/L free cytosolic Ca^{2+}). **B,** Comparison of RyR2 open probability in Ctl and POAF in the absence or presence of simulated IL-1β application. Simulated effects of IL-1β included a 25% increase in RyR2 open probability based on experimental data showing increased Ca^{2+}-spark frequency during IL-1β application.[30]

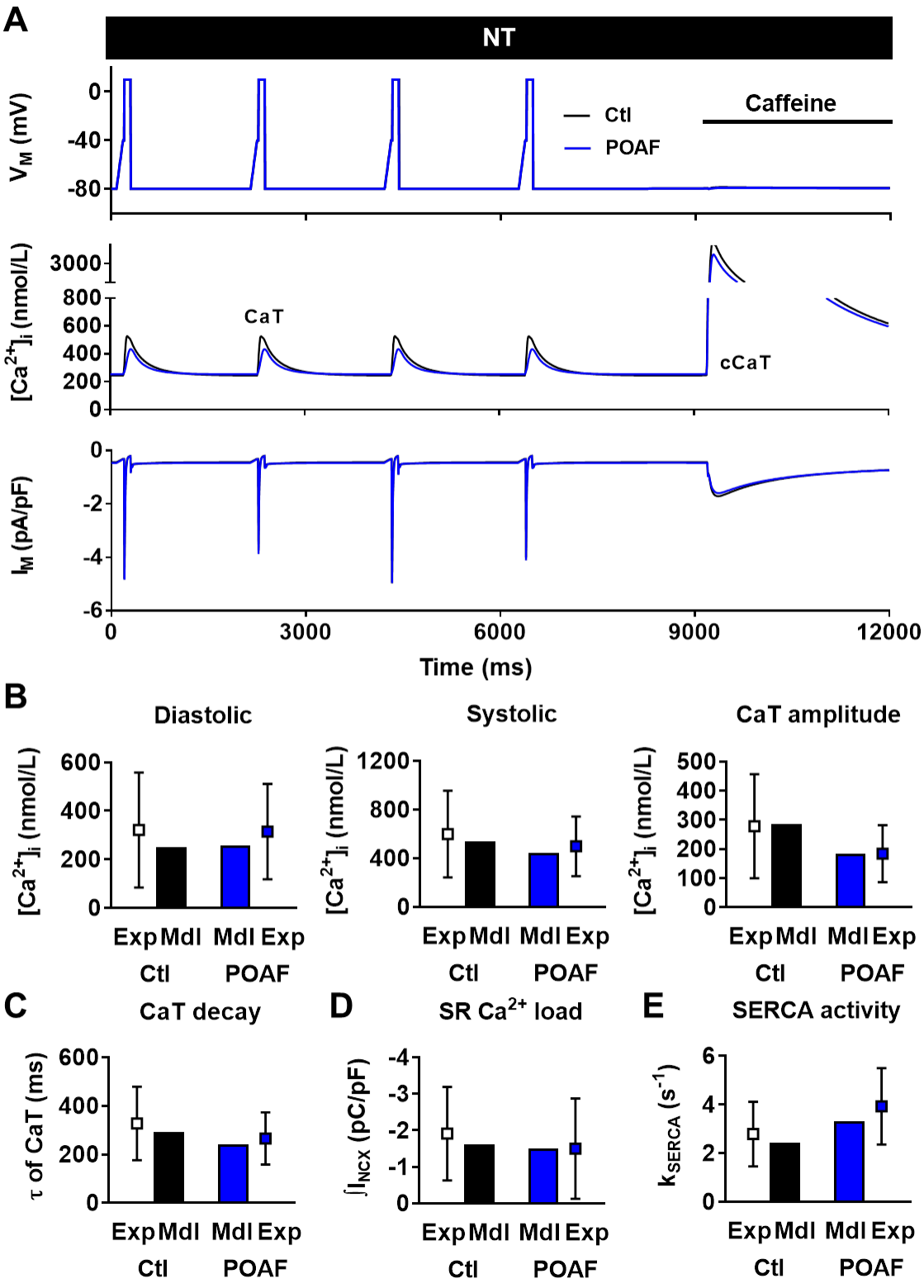

Online Figure XVI. Validation of computational models. A, Simulated voltage-clamp protocol (top), whole-cell Ca^{2+} transient (CaT, middle) and total membrane current (bottom) in Ctl and POAF model variants. **B-E,** Comparison of diastolic and systolic Ca^{2+} levels, and CaT amplitude (**B**), time constant (τ) of CaT decay (**C**), sarcoplasmic reticulum (SR) Ca^{2+} load measured as integrated NCX current (I_{NCX}) during the caffeine-induced CaT (cCaT, **D**), and SERCA activity estimated as the difference in decay rates between the CaT and cCaT (**E**), in Ctl and POAF model variants (bars) with experimental data (symbols).

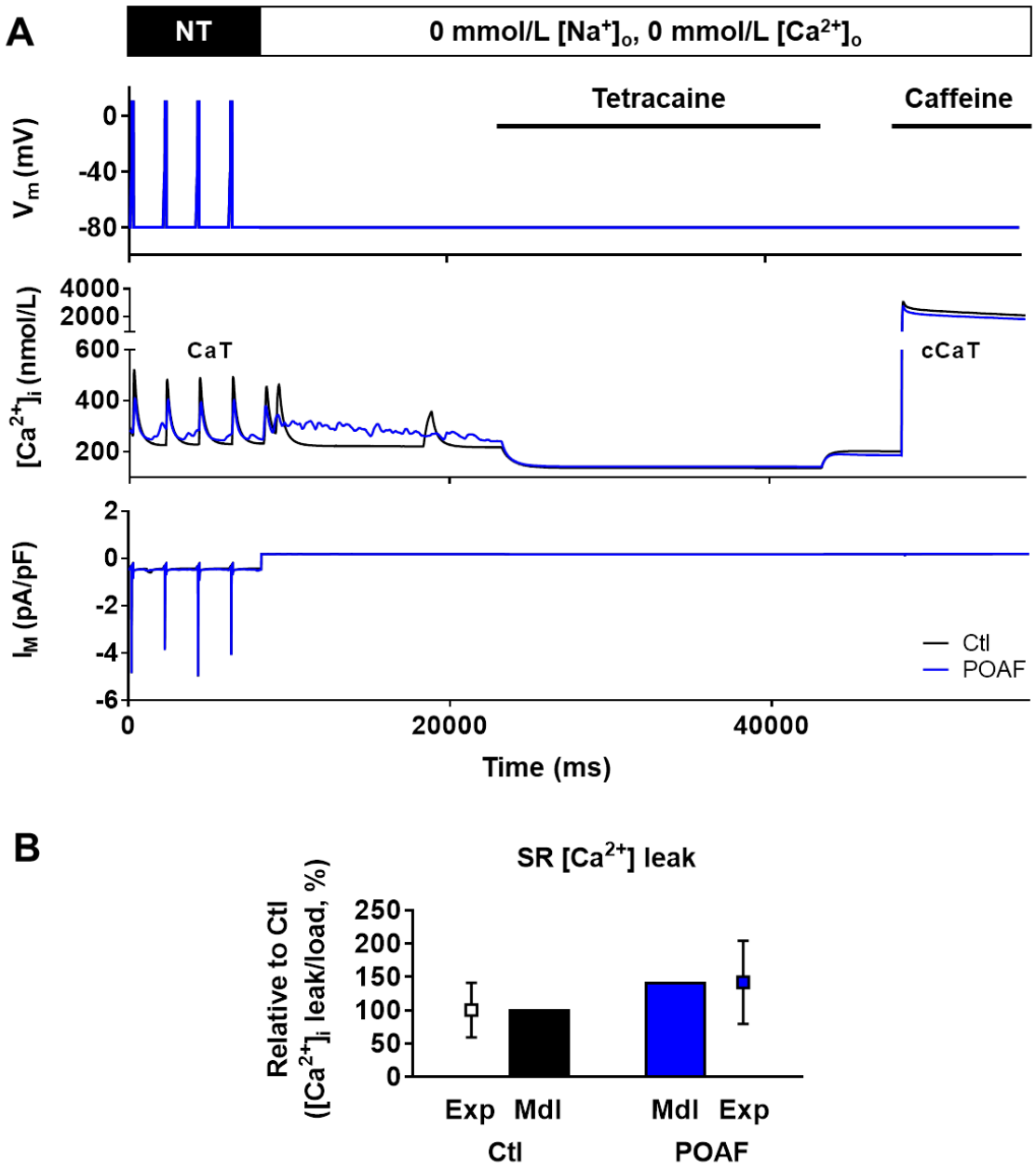

Online Figure XVII. Simulated sarcoplasmic reticulum (SR) Ca^{2+} leak protocol in Ctl and POAF model variants. A, Voltage-clamp protocol (**top**), whole-cell Ca^{2+} (**middle**) and membrane current (**bottom**) during simulated application of the Shannon protocol[8] to measure SR Ca^{2+}-leak and SR Ca^{2+}-load. The effects of tetracaine and caffeine were simulated by blocking RyR2 by >99% and setting RyR2 open probability to 1.0, respectively. SR Ca^{2+}-leak was quantified as the decrease in cytosolic Ca^{2+} during tetracaine application and SR Ca^{2+}-load was quantified as the amplitude of the caffeine-induced Ca^{2+} transient (CaT). **B,** Relative (load normalized) SR Ca^{2+}-leak in Ctl and POAF compared to experimental data from **Figure 3A**.

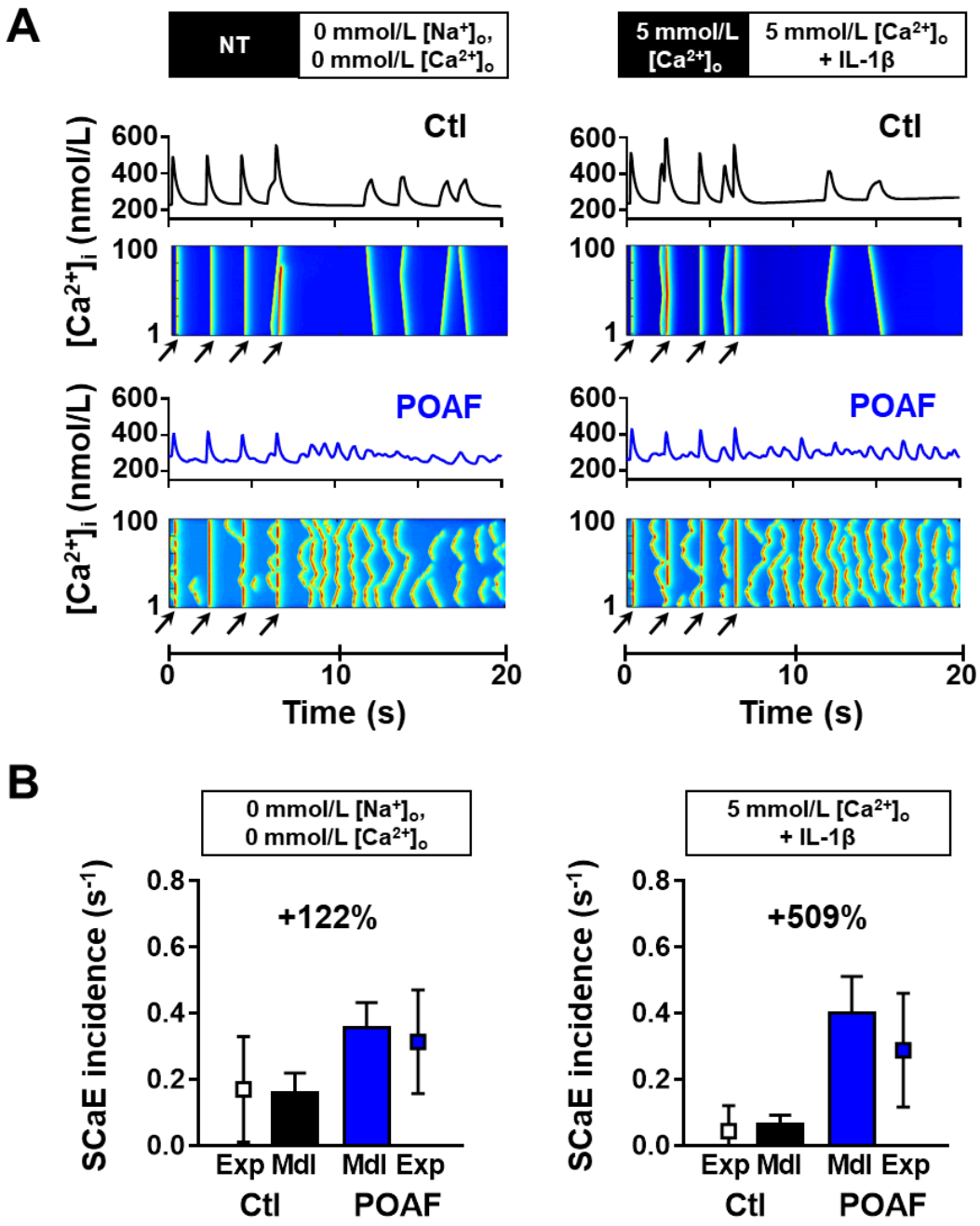

Online Figure XVIII. Simulated sarcoplasmic reticulum (SR) Ca^{2+}-release evens (SCaEs) in Ctl and POAF model variants under different conditions. A, Whole-cell Ca^{2+}-transient (CaT) and longitudinal line-scan of depolarization-induced CaTs (arrows) or SCaEs in Ctl (top row) and POAF (bottom row) models under voltage-clamp conditions with 0-mmol/L Na^+/0-mmol/L Ca^{2+} (left; experimental conditions in **Figure 3B-C**) or 5-mmol/L Ca^{2+} followed by acute application of IL-1β (experimental conditions in **Figure 7B-D**). **B,** Validation of SCaE-incidence in both model variants (bars) compared to experimental data obtained under the same condition (symbols).

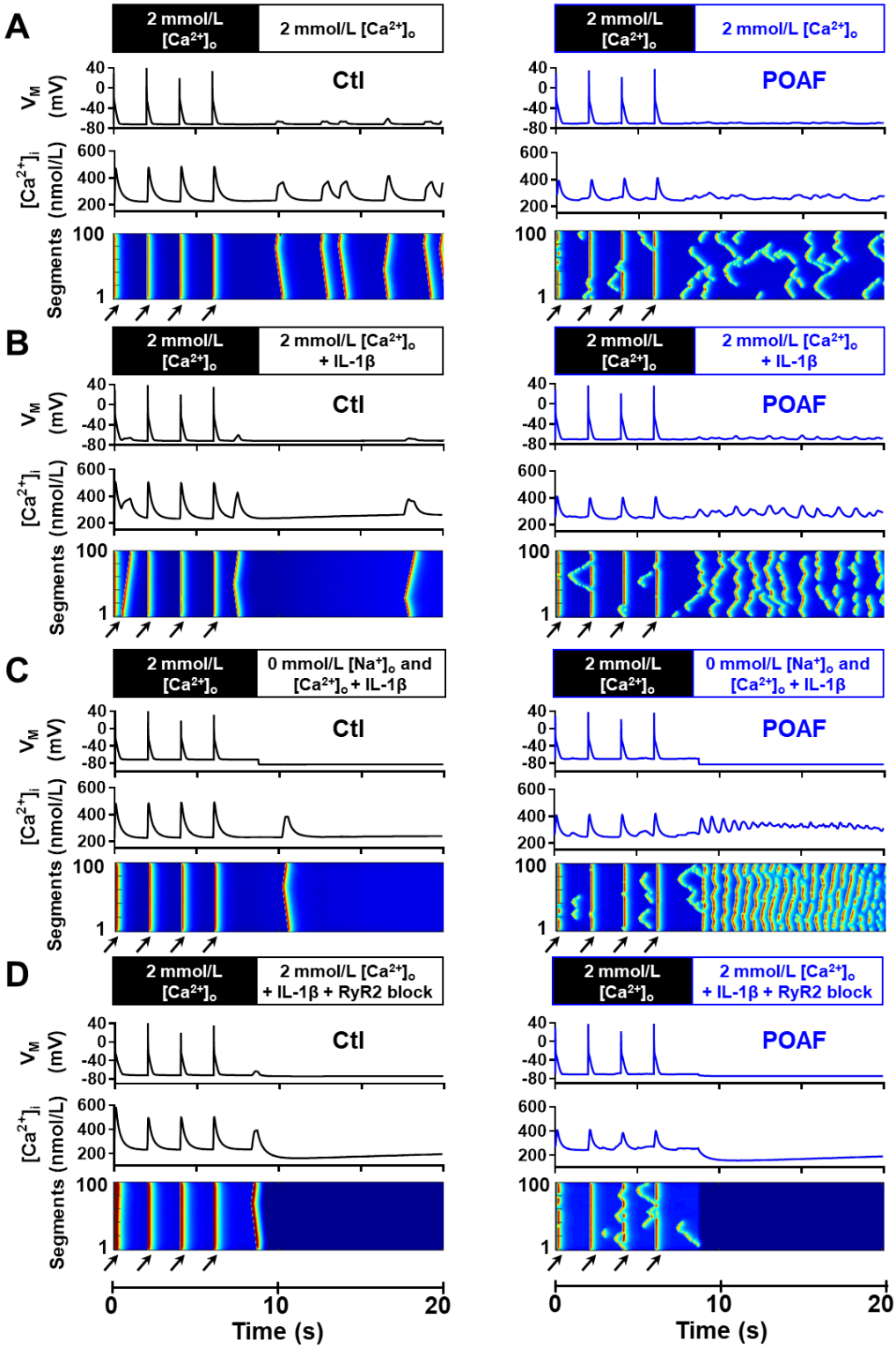

Online Figure XIX. Current-clamp simulations during 0.5-Hz pacing (arrows) and post-pacing follow-up period to assess spontaneous sarcoplasmic reticulum Ca^{2+}-release events (SCaEs) and corresponding delayed afterdepolarizations (DADs) in the Ctl (left) and POAF (right) model variants. A, Membrane potential (V_M, top), whole-cell Ca^{2+}-transient (middle) and longitudinal line scan through the center of the virtual cardiomyocyte (bottom) under control conditions (2-mmol/L extracellular Ca^{2+}). **B,** Similar to panel A in the presence of simulated IL-1β application during the follow-up. **C,** Similar to panel B, but in the absence of extracellular Na^+ and Ca^{2+} to inhibit transmembrane Ca^{2+} fluxes. **D,** Similar to panel B with inhibition of ryanodine receptor channel type-2 (RyR2)-mediated Ca^{2+} release.

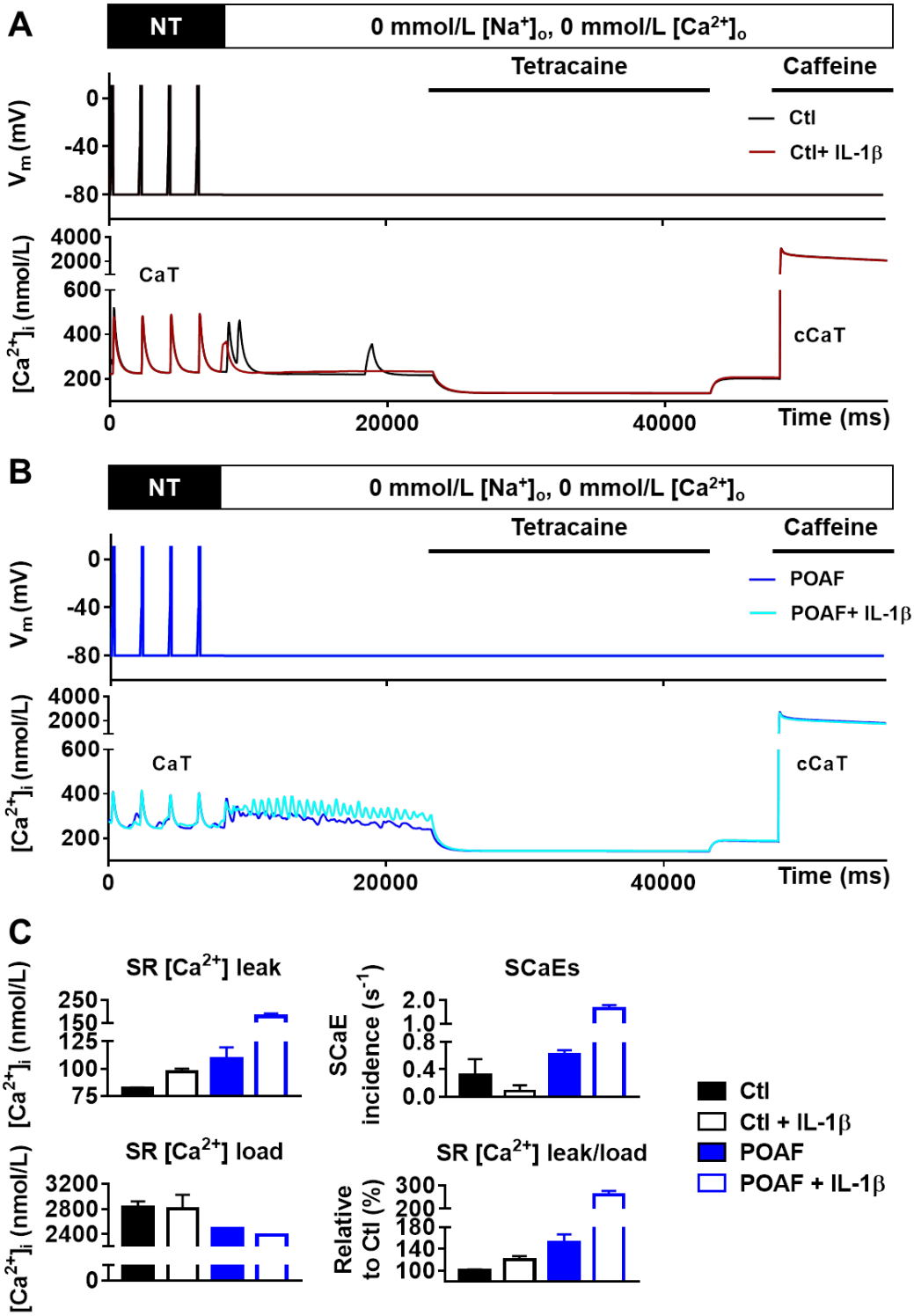

Online Figure XX. Simulated sarcoplasmic reticulum (SR) Ca^{2+}-leak protocol in the absence or presence of interleukin-1β (IL-1β) stimulation. A, Voltage-clamp protocol (**top**) and whole-cell Ca^{2+} (**bottom**) during simulated application of the Shannon protocol[36] to measure SR Ca^{2+}-leak and SR Ca^{2+}-load in the Ctl model in the absence (black line) or presence (red line) of IL-1β. The effects of tetracaine and caffeine were simulated by blocking RyR2 by more than 99% and setting RyR2 open probability to 1.0, respectively. **B,** Similar to panel A for the POAF model version. **C, Top**: Quantification of SR Ca^{2+}-leak and incidence of spontaneous SR Ca^{2+}-release events (SCaEs). **Bottom**: SR Ca^{2+}-load (amplitude of the caffeine-induced Ca^{2+} transient, CaT) and SR Ca^{2+}-leak/load in Ctl and POAF with and without IL-1β stimulation.

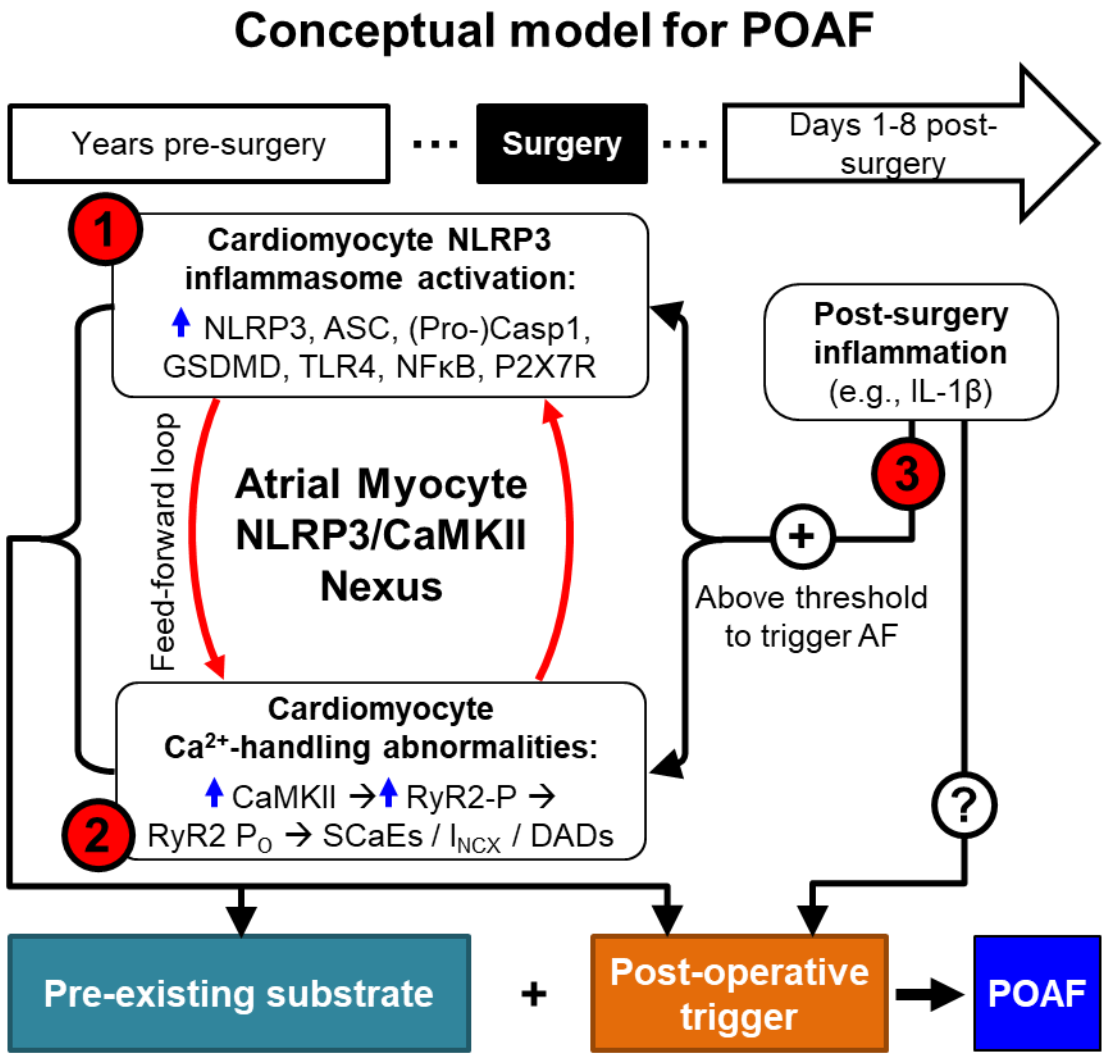

Online Figure XXI. Major findings and conceptual model for post-operative atrial fibrillation (POAF). Patients that go on to develop POAF have a pre-existing substrate characterized by (1) Increased cardiomyocyte NLRP3-inflammasome activation and (2) CaMKII-dependent, RyR2-mediated cardiomyocyte Ca^{2+}-handling abnormalities. In addition, (3) post-surgery inflammation (e.g., acute IL-1β releases) further activates the atrial NLRP3-inflammasome and exacerbates CaMKII-dependent Ca^{2+}-handling abnormalities. Taken together, these data support a novel model in which the post-surgical IL-1β-induced increases in phosphorylation levels of Ca^{2+}-handling proteins exacerbate the pre-existing SR dysfunction, reaching a value above the threshold needed to cause potentially proarrhythmic SCaEs and DADs that might predispose to POAF development. These observations provide a unifying model of AF that accounts for the high long-term AF recurrence-rate in POAF patients as well as the transient occurrence of POAF post-operatively.

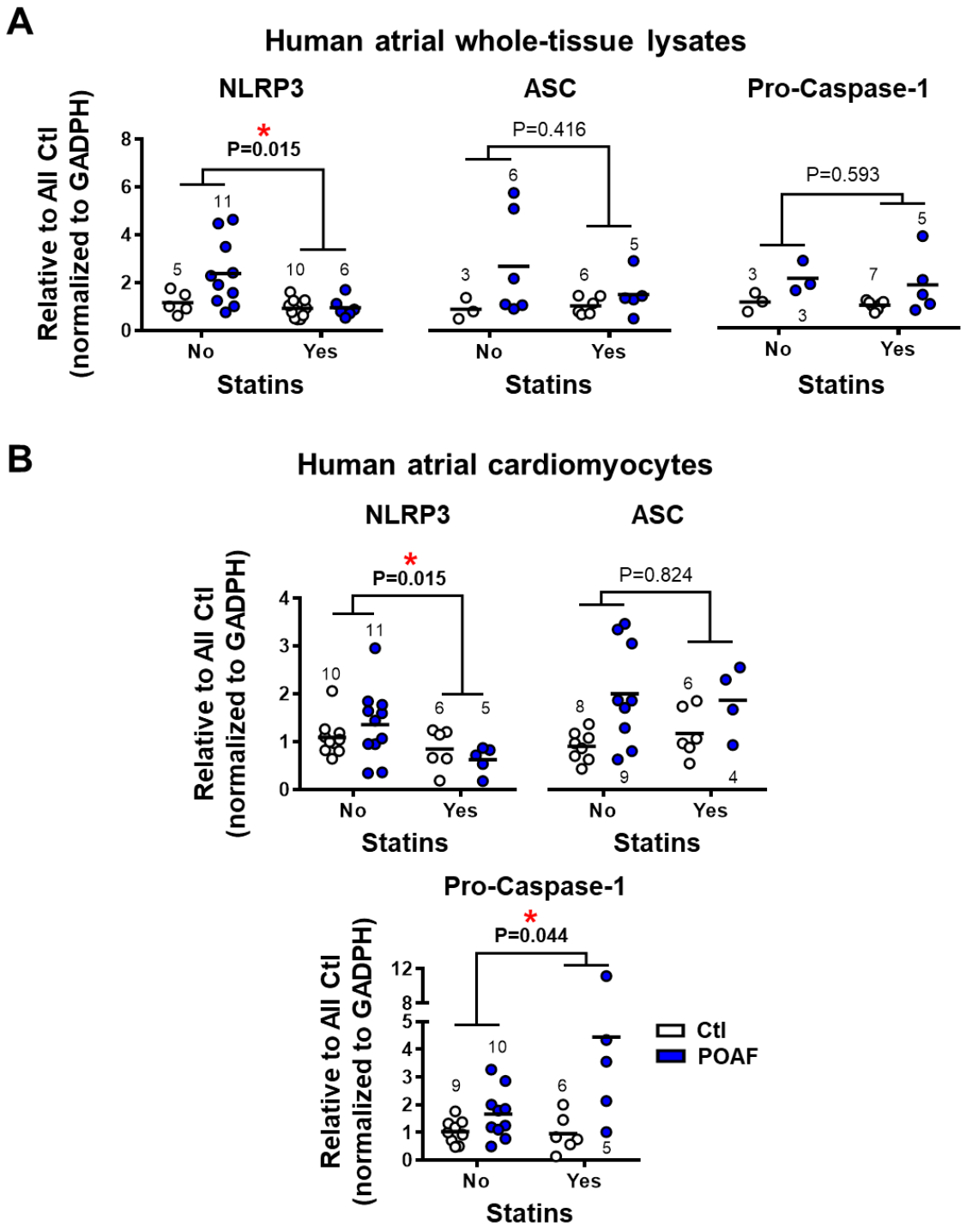

Online Figure XXII. Dependence of atrial NACHT, LRR, and PYD domains containing protein-3 (NLRP3) inflammasome components on statin use and post-operative rhythm. Protein levels of NLRP3, apoptosis-associated speck-like protein containing a CARD (ASC), and Pro-caspase-1 in atrial whole-tissue lysates (**A**) or human atrial cardiomyocytes (**B**) of Ctl and POAF patients who did (Yes) or did not (No) use lipid-lowering drugs. Numbers above or below symbols indicate number of patients. **P*<0.05 for the factor 'statin use' based on two-way ANOVA. Note that individual subgroups may be small, limiting the statistical power and robustness of these subanalyses.

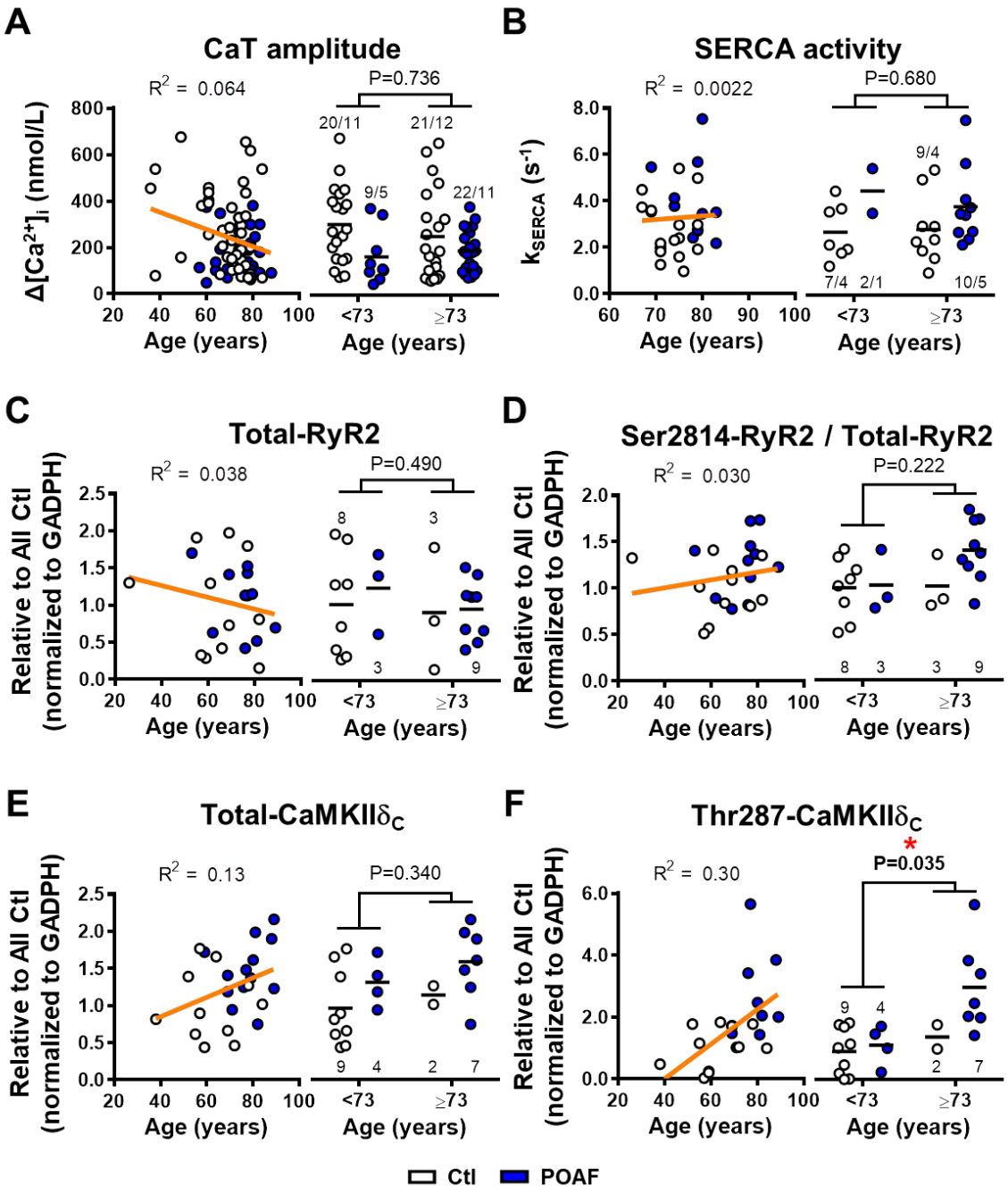

Online Figure XXIII. Age and rhythm dependence of Ca^{2+}-handling parameters. Correlation between parameter value and age, with corresponding correlation coefficients (R^2; **left**) and parameter values in Ctl and POAF patients <73 years vs. ≥73 years (**right**). **A**, Ca^{2+}-transient (CaT) amplitude. **B,** Sarcoplasmic reticulum Ca^{2+}-ATPase (SERCA) activity. **C,** Total ryanodine receptor channel type-2 (RyR2) protein levels. **D,** Relative Ser2814-RyR2 phosphorylation levels. **E,** Total cytosolic Ca^{2+}/calmodulin-dependent protein kinase-IIδ ($CaMKII\delta_C$) protein levels. **F,** $CaMKII\delta_C$ autophosphorylation levels at Thr287. Numbers above or below symbols indicate number of cardiomyocytes/patients (panels **A-B**) or patients (panels **C-F**). **P*<0.05 for the factor 'age' based on two-way ANOVA. Note that individual subgroups may be small, limiting the statistical power and robustness of these subanalyses.

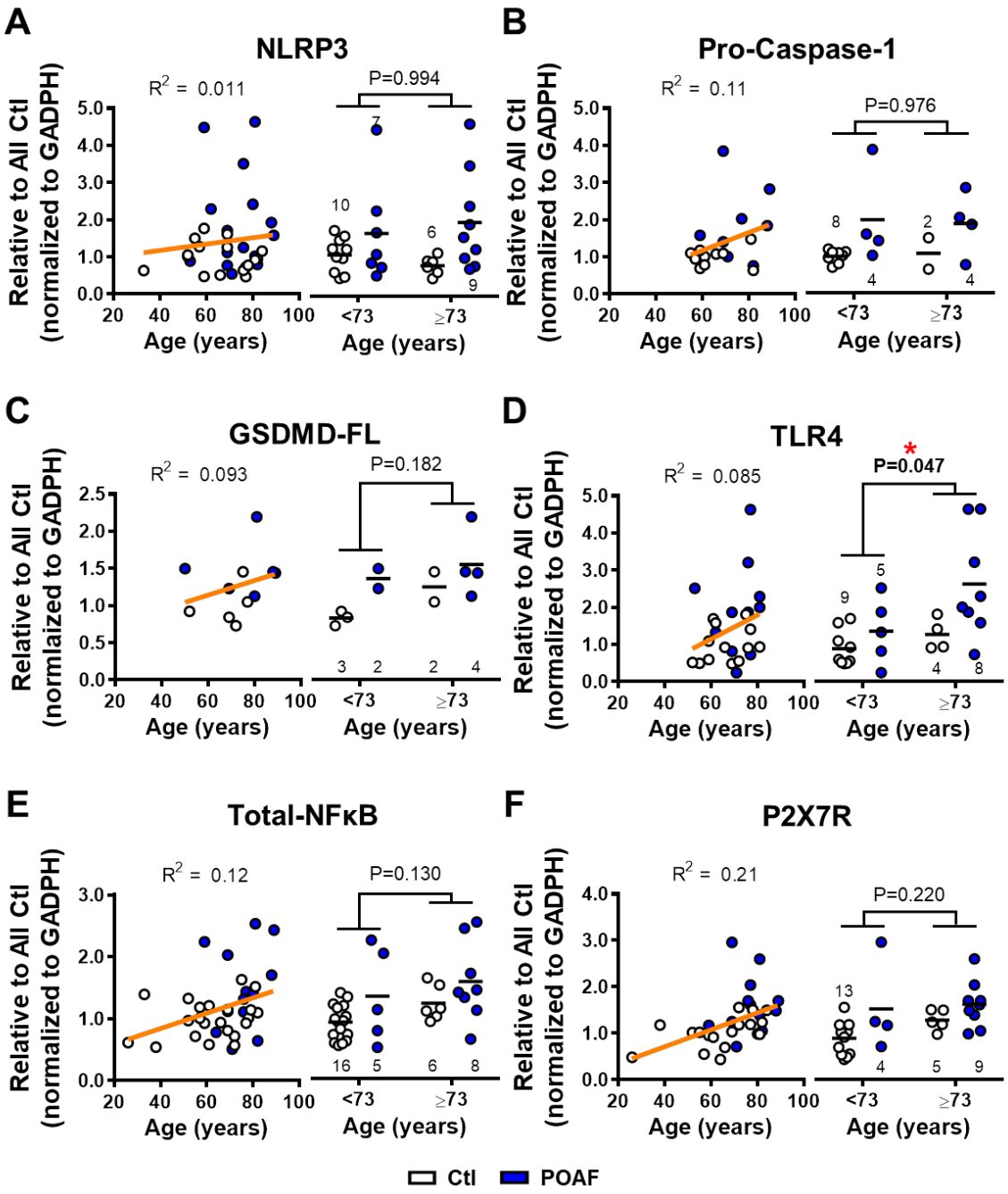

Online Figure XXIV. Age and rhythm dependence of atrial NACHT, LRR, and PYD domains containing protein-3 (NLRP3) inflammasome parameters. Correlation between parameter value and age, with corresponding correlation coefficients (R^2; **left**) and parameter values in Ctl and POAF patients <73 years vs. ≥73 years (**right**). **A**, NLRP3 protein levels. **B,** Pro-caspase1 protein levels. **C,** Full-length gasdermin-D (GSDMD-FL) protein levels. **D,** Toll-like receptor-4 protein levels. **E,** Total nuclear factor kappa-light-chain-enhancer of activated B cells (NFκB) protein levels. **F,** purinergic P2X7 receptor (P2X7R) protein levels. Numbers above or below symbols indicate number of patients. **P*<0.05 for the factor 'age' based on two-way ANOVA. Note that individual subgroups may be small, limiting the statistical power and robustness of these subanalyses.

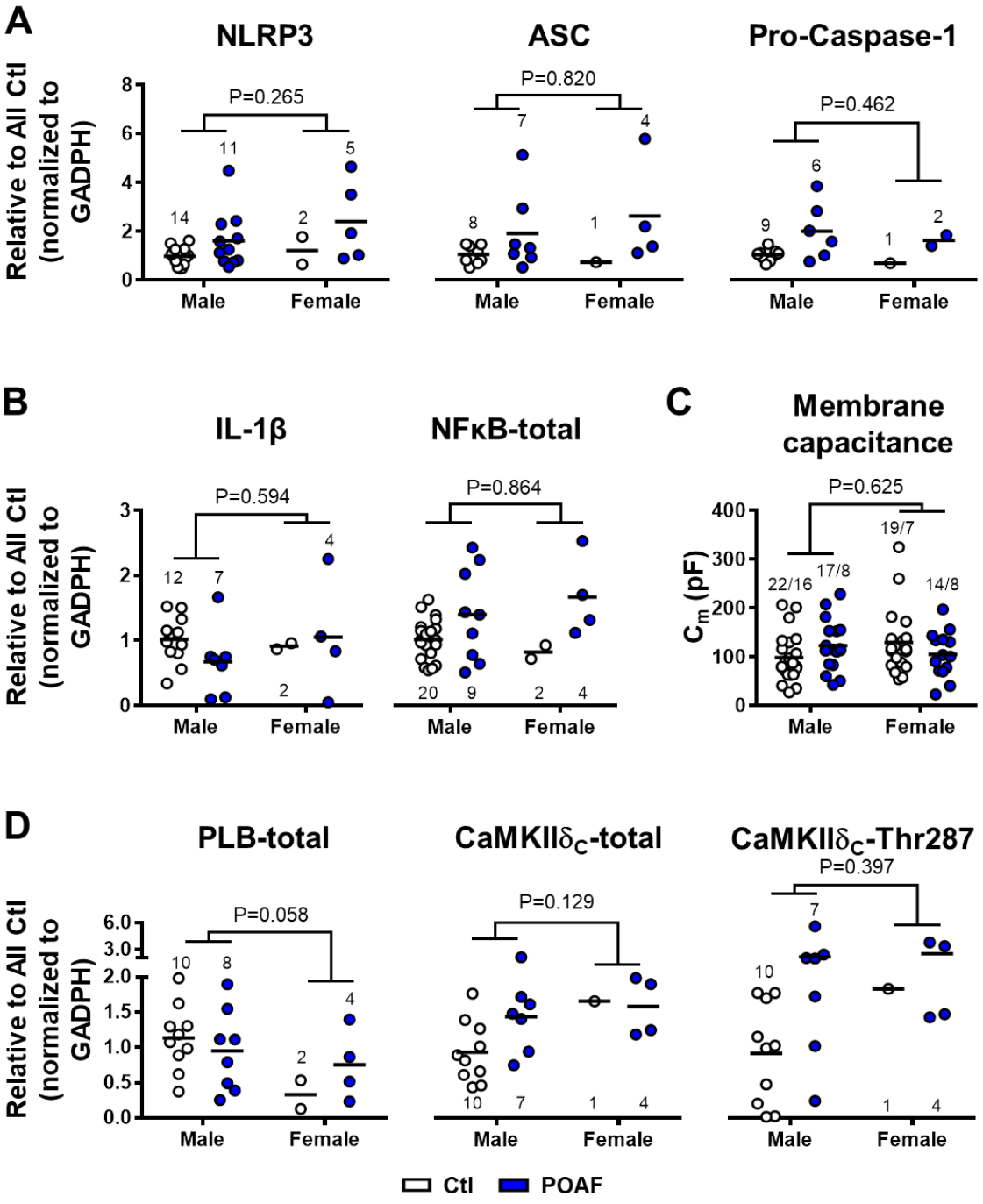

595 **Online Figure XXV. Relationship between sex and NLRP3 inflammasome activation or Ca^{2+}-handling changes. A-D,** Two-way ANOVA analysis of post-operative rhythm status and sex (male vs. female) for NACHT, LRR, and PYD domains containing protein 3 (NLRP3), apoptosis-associated speck-like protein containing a CARD (ASC) and pro-Caspase-1 (panel **A**), interleukin-1β (IL-1β) and total nuclear factor kappa-B (NFκB, panel
600 **B**), cardiomyocyte membrane capacitance (C_m, panel **C**), and total phospholamban (PLB) or total/Thr287-phosphorylated Ca^{2+}/calmodulin-dependent protein kinase-IIδ_C (CaMKIIδ_C. panel **D**) protein levels. P values reflect significance level of the factor 'sex' in two-way ANOVA. Note that individual subgroups may be small, limiting the statistical power and robustness of these subanalyses.

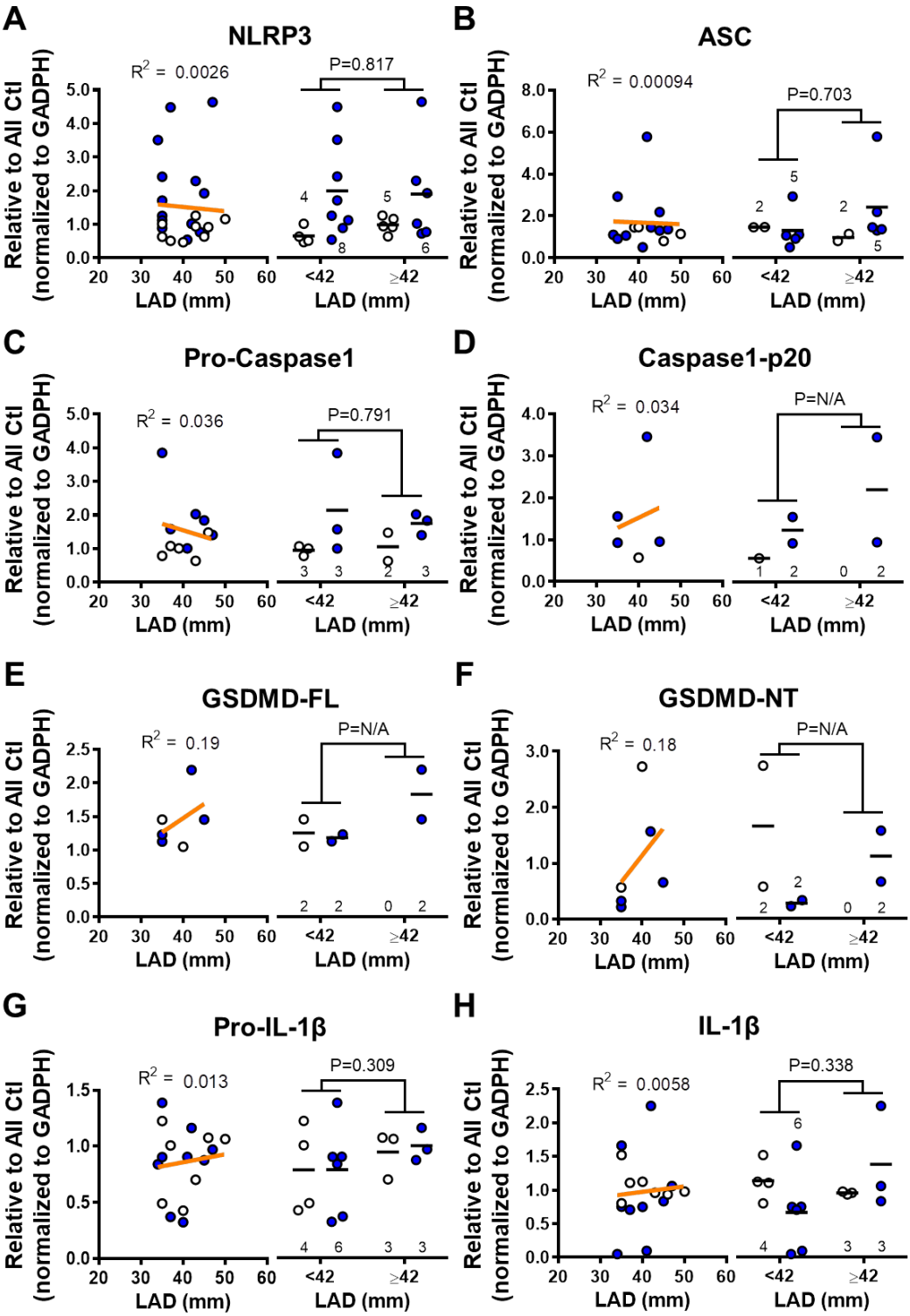

Online Figure XXVI. Relationship between left atrial diameter (LAD) and NLRP3-inflammasome protein levels. Left panels show correlation between LAD and protein levels of NLRP3-inflammasome components/products. Right panels show two-way ANOVA analysis of post-operative rhythm and LAD (with a threshold of 42 mm). P values reflect significance level of the factor 'LAD'. N-numbers indicate number of patients. **P*<0.05. **A,** NACHT, LRR, and PYD domains containing protein 3 (NLRP3). **B,** Apoptosis-associated speck-like protein containing a CARD (ASC). **C-D.** Pro-Caspase-1 (C) and its active 20 kDa fragment (D). **E-F,** Full-length (E) and pore-forming N-terminal (F) gasdermin-D (GSDMD). **G-H.** (Pro-)interleukin-1β (IL-1β). Note that individual subgroups may be small, limiting the statistical power and robustness of these subanalyses.

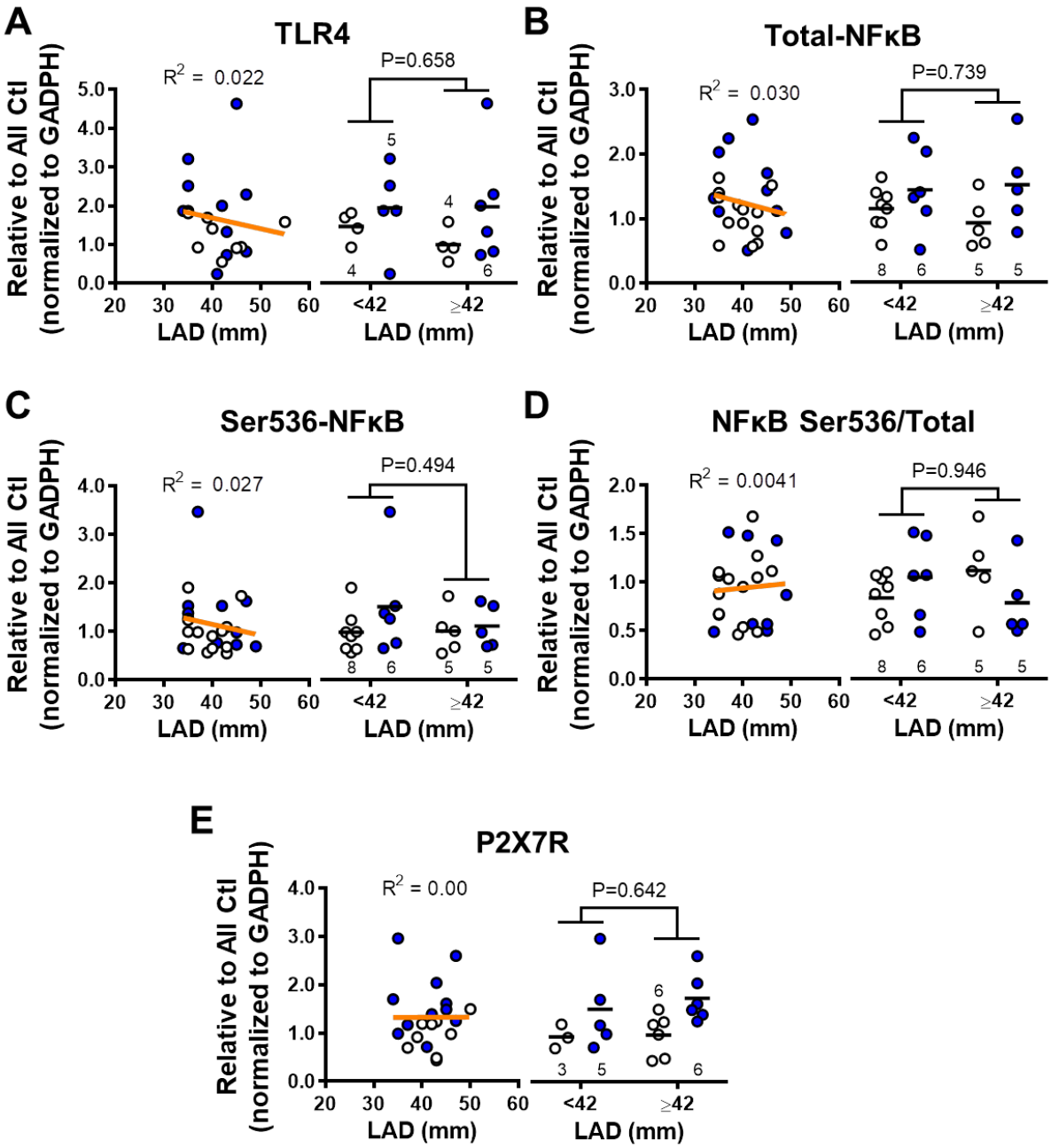

Online Figure XXVII. Relationship between left atrial diameter (LAD) and components involved in priming and triggering of the NLRP3-inflammasome. Left panels show correlation between LAD and individual parameters. Right panels show two-way ANOVA analysis of post-operative rhythm and LAD (with a threshold of 42 mm). P values reflect significance level of the factor 'LAD'. N-numbers indicate number of patients. *P<0.05. **A,** Toll-like receptor-4 protein levels. **B-D,** Total (B), Ser536-phosphorylated (C) and relative (phosphorylated / total, D) nuclear factor kappa-B protein levels. **E,** P2X7 receptor protein levels. Note that individual subgroups may be small, limiting the statistical power and robustness of these subanalyses.

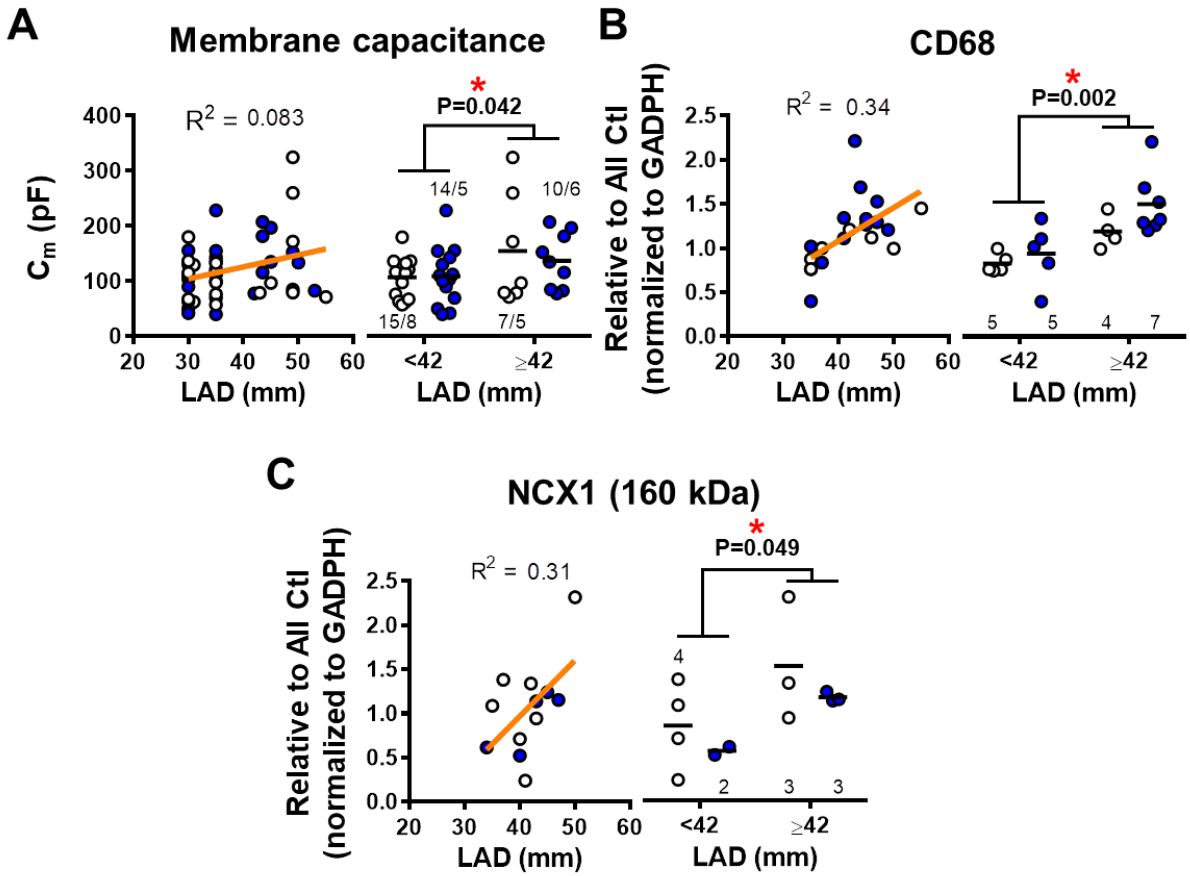

Online Figure XXVIII. Parameters correlating with left atrial diameter (LAD). Left panels show correlation between LAD and individual parameters. Right panels show two-way ANOVA analysis of post-operative rhythm and LAD (with a threshold of 42 mm). P values reflect significance level of the factor 'LAD'. **P*<0.05. **A,** Cardiomyocyte membrane capacitance (C_m). **B,** Macrophage marker CD68. **C,** Full-length (160 kDa) variant of the Na^+/Ca^{2+}-exchanger type-1 (NCX1). N-numbers indicate cells/patients (panel A), or patients (panels B-C). Note that individual subgroups may be small, limiting the statistical power and robustness of these subanalyses.

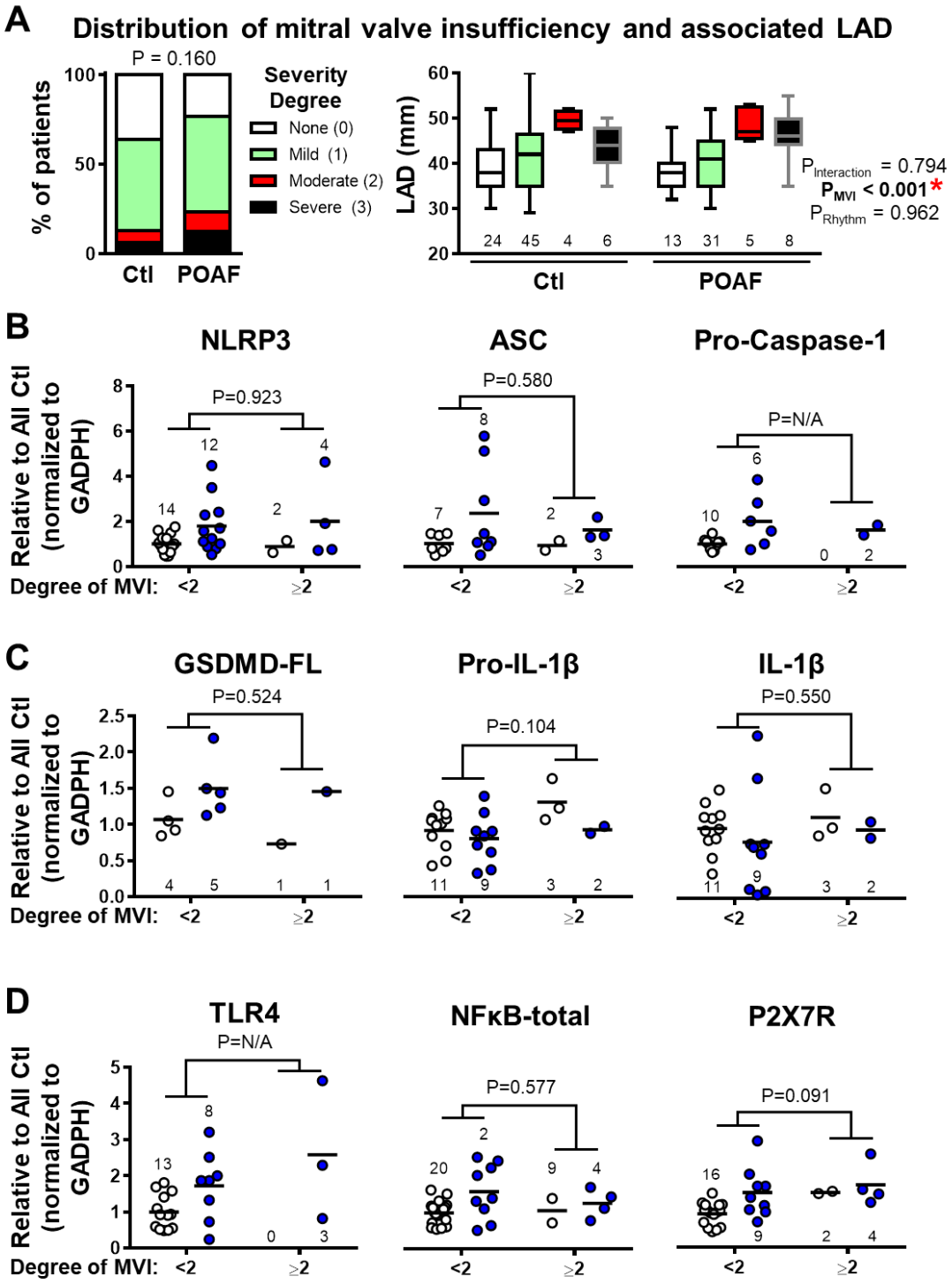

Online Figure XXIX. Relationship between mitral valve insufficiency (MVI) and NLRP3 inflammasome activation. A, Distribution of the degree of MVI in Ctl (n=114) and POAF (n=73) and association between MVI (Left-to-right: none, mild, moderate or severe) and LAD. Numbers below indicate number of patients in each category for whom LAD was available. **B-D,** Two-way ANOVA analysis of post-operative rhythm status and MVI (none/mild vs. moderate/severe) for NACHT, LRR, and PYD domains containing protein 3 (NLRP3), apoptosis-associated speck-like protein containing a CARD (ASC) and pro-Caspase-1 (panel **B**), full-length gasdermin-D, pro-interleukin-1β and interleukin-1β (panel **C**), toll-like receptor-4 (TLR4), total nuclear factor kappa-B and P2X7 receptor (panel **D**) protein levels. P values reflect significance level of the factor 'MVI' in two-way ANOVA. Note that individual subgroups may be small, limiting the statistical power and robustness of these subanalyses.

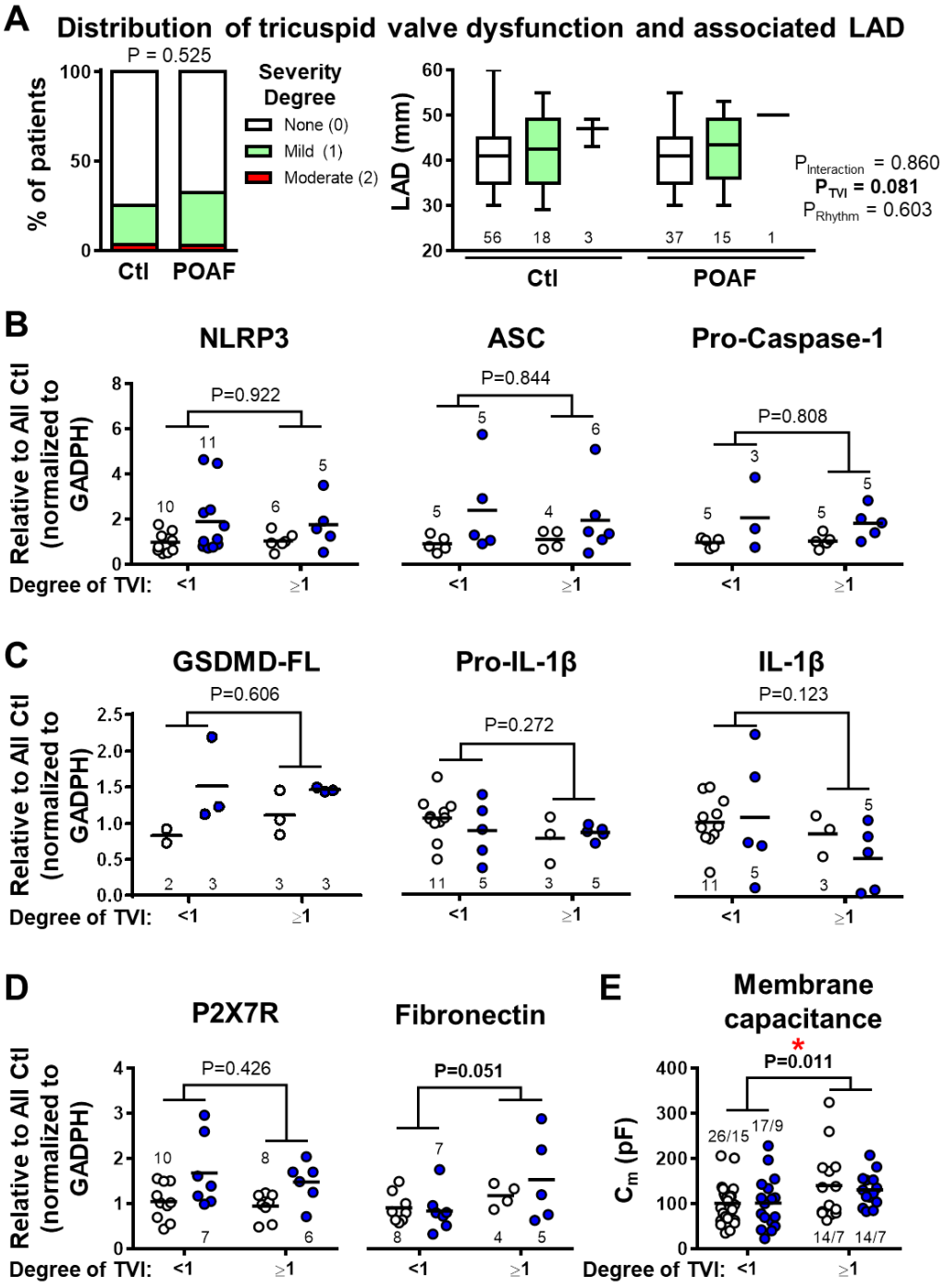

Online Figure XXX. Relationship between tricuspid valve insufficiency (TVI) and NLRP3 inflammasome activation. A, Distribution of the degree of TVI in Ctl (n=111) and POAF (n=65) and association between TVI (Left-to-right: none, mild or moderate) and LAD. Numbers below indicate number of patients in each category for whom LAD was available. **B-D,** Two-way ANOVA analysis of post-operative rhythm status and TVI (none vs. mild/moderate) for NACHT, LRR, and PYD domains containing protein 3 (NLRP3), apoptosis-associated speck-like protein containing a CARD (ASC), and pro-Caspase-1 (panel **B**), full-length gasdermin-D, pro-interleukin-1β and interleukin-1β (panel **C**), as well as P2X7 receptor and fibronectin protein levels (panel **D**). **E,** Two-way ANOVA analysis of post-operative rhythm status and TVI (none vs. mild/moderate) for cardiomyocyte membrane capacitance (C_m). N-numbers indicate number of cells/patients (panel E) or patients (other panels). P values reflect significance level of the factor 'TVI' in two-way ANOVA. Note that individual subgroups may be small, limiting the statistical power and robustness of these subanalyses.

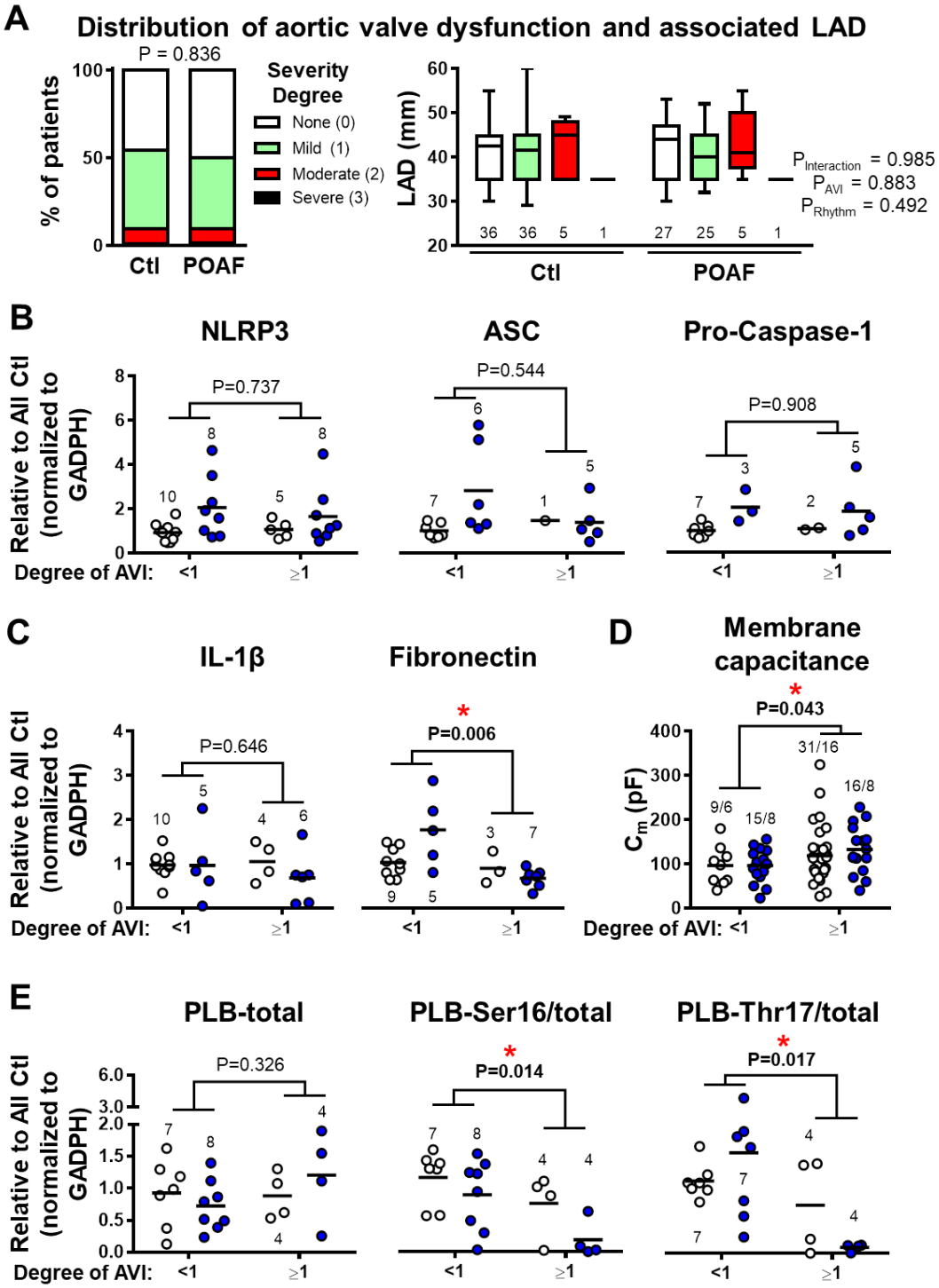

Online Figure XXXI. Relationship between aortic insufficiency (AVI) and NLRP3 inflammasome activation. A, Distribution of the degree of AVI in Ctl (n=116) and POAF (n=74) and association between AVI (Left-to-right: none, mild, moderate or severe) and LAD. Numbers below indicate number of patients in each category for whom LAD was available. **B-E,** Two-way ANOVA analysis of post-operative rhythm status and AVI (none vs. mild/moderate/severe) for NACHT, LRR, and PYD domains containing protein 3 (NLRP3), apoptosis-associated speck-like protein containing a CARD (ASC), and pro-Caspase-1 (panel **B**), interleukin-1β (IL-1β) and fibronectin (panel **C**), membrane capacitance (C_m; **D**), and total, Ser16-phosphorylated, or Thr17-phosphorylated phospholamban (PLB; panel **E**). N-numbers indicate number of cells/patients (panel D) or patients (other panels). P values reflect significance level of the factor 'AVI' in two-way ANOVA. Note that individual subgroups may be small, limiting the statistical power and robustness of these subanalyses.

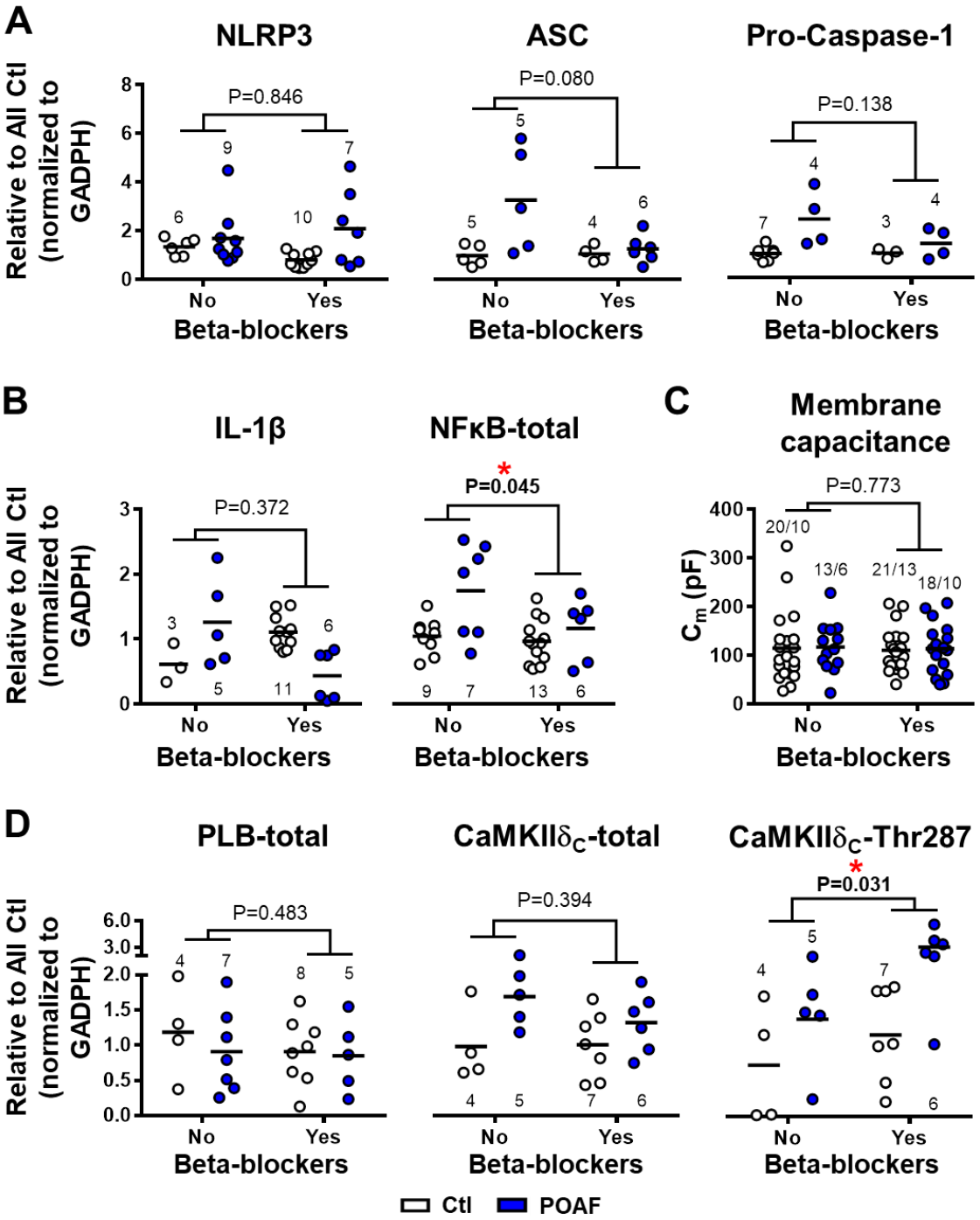

Online Figure XXXII. Relationship between beta-blocker use and NLRP3 inflammasome activation or Ca^{2+}-handling changes. A-D, Two-way ANOVA analysis of post-operative rhythm status and beta-blocker use (no vs. yes) for NACHT, LRR, and PYD domains containing protein 3 (NLRP3), apoptosis-associated speck-like protein containing a CARD (ASC) and pro-Caspase-1 (panel **A**), interleukin-1β (IL-1β) and total nuclear factor kappa-B (NFκB, panel **B**), cardiomyocyte membrane capacitance (C_m, panel **C**), and total phospholamban (PLB) or total/Thr287-phosphorylated Ca^{2+}/calmodulin-dependent protein kinase-IIδ_C (CaMKIIδ_C. panel **D**) protein levels. P values reflect significance level of the factor 'beta-blockers' in two-way ANOVA. Note that individual subgroups may be small, limiting the statistical power and robustness of these subanalyses.

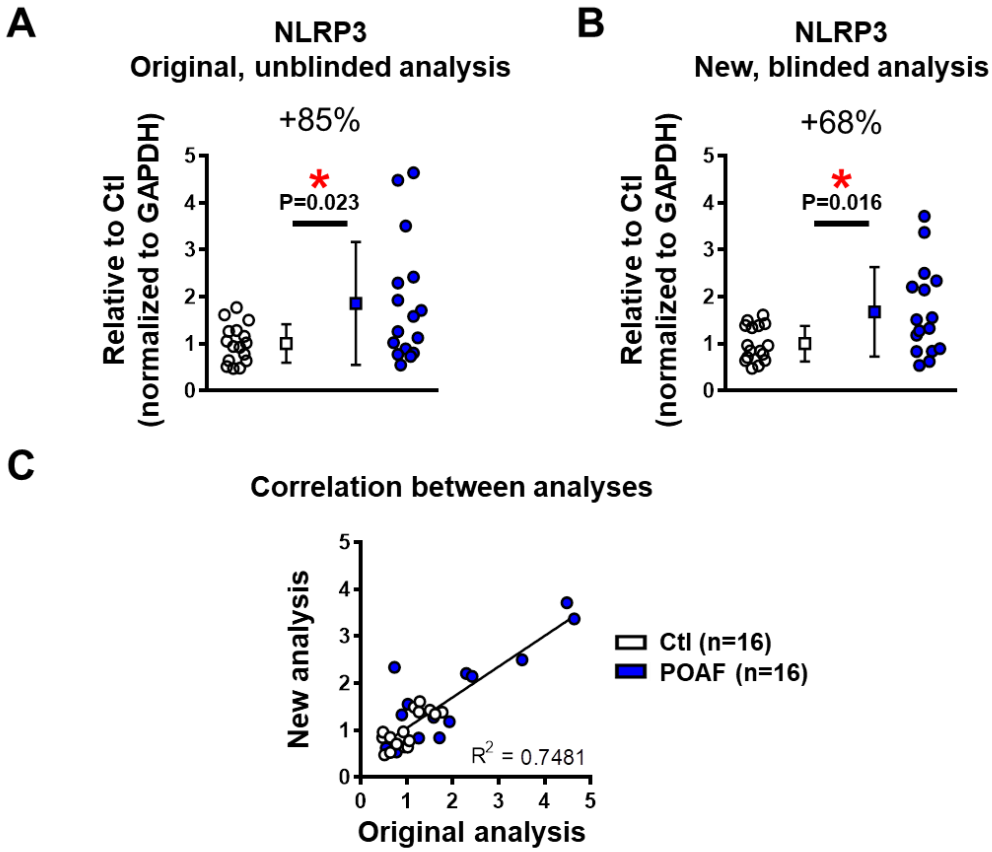

D

Protein	n-numbers	POAF vs. Ctl Original, unblinded analysis	POAF vs. Ctl New, blinded analysis	Correlation coefficient
NLRP3 (tissue)	16 vs. 16	+85% (P=0.023)	+68% (P=0.016)	0.748
Pro-Casp1 (CMs)	15 vs. 15	+159% (P=0.006)	+205% (P=0.024)	0.898
Casp1-p37 (CMs)	15 vs. 15	+311% (P<0.001)	+464% (P=0.008)	0.837
GSDMD-FL (tissue)	5 vs. 6	+49% (P=0.030)	+27% (P=0.144)	0.626
GSDMD-FL (CMs)	12 vs. 9	+140% (P=0.041)	+142% (P=0.032)	0.748
GSDMD-NT (CMs)	12 vs. 9	+298% (P=0.008)	+294% (P=0.002)	0.676
P2X7R (tissue)	18 vs. 13	+59% (P=0.008)	+60% (P=0.011)	0.793
RyR2-total (tissue)	11 vs. 12	+4% (P=0.884)	+2% (P=0.950)	0.988
RyR2-S2814/tot (tissue)	11 vs. 12	+31% (P=0.040)	+36% (P=0.019)	0.969
CaMKIIδc-tot (tissue)	11 vs. 11	+49% (P=0.019)	+47% (P=0.070)	0.527
CaMKIIδc-Thr287/tot (tissue)	11 vs. 11	+60% (P=0.166)	+42% (P=0.264)	0.769
			Average	0.78±0.14

Online Figure XXXIII. Comparison between the original unblinded Western blot analysis and the independent re-analysis blinded to postoperative rhythm outcome performed during the revision. A-B. Quantification of NLRP3 proteins levels in human atrial whole-tissue homogenates of Ctl (white symbols) and POAF (blue symbols) patients during the original unblinded analysis (**A**) and the new analysis blinded to post-operative rhythm outcome (**B**). *P<0.05 vs. Ctl based on Student's *t*-test with Welch's correction for unequal variance. **C.** Correlation between relative NLRP3 protein levels from both analyses for individual Ctl and POAF samples. **D.** Overview of n-numbers, relative differences between POAF and Ctl in the original, unblinded analysis and in the new, blinded analysis, as well as correlation coefficients between the original and new analyses, for different Western blot results.